Cellular and Molecular Life Sciences (2020) 77:4957–4976
https://doi.org/10.1007/s00018-019-03442-5

ORIGINAL ARTICLE

GRK2 levels in myeloid cells modulate adipose-liver crosstalk in high fat diet-induced obesity

Rocío Vila-Bedmar[1] · Marta Cruces-Sande[2,3,4] · Alba C. Arcones[2,3,4] · Hanneke L. D. M. Willemen[5] · Patricia Prieto[4,6] · Isabel Moreno-Indias[7,8] · Daniel Díaz-Rodríguez[2] · Sara Francisco[2] · Rafael I. Jaén[6] · Carolina Gutiérrez-Repiso[7,8] · Cobi J. Heijnen[9] · Lisardo Boscá[4,6] · Manuel Fresno[2,3] · Annemieke Kavelaars[9] · Federico Mayor Jr[2,3,4] · Cristina Murga[2,3,4]

Received: 26 July 2019 / Revised: 18 December 2019 / Accepted: 23 December 2019 / Published online: 11 January 2020

Abstract

Macrophages are key effector cells in obesity-associated inflammation. G protein-coupled receptor kinase 2 (GRK2) is highly expressed in different immune cell types. Using LysM-GRK2$^{+/-}$ mice, we uncover that a reduction of GRK2 levels in myeloid cells prevents the development of glucose intolerance and hyperglycemia after a high fat diet (HFD) through modulation of the macrophage pro-inflammatory profile. Low levels of myeloid GRK2 confer protection against hepatic insulin resistance, steatosis and inflammation. In adipose tissue, pro-inflammatory cytokines are reduced and insulin signaling is preserved. Macrophages from LysM-GRK2$^{+/-}$ mice secrete less pro-inflammatory cytokines when stimulated with lipopolysaccharide (LPS) and their conditioned media has a reduced pathological influence in cultured adipocytes or naïve bone marrow-derived macrophages. Our data indicate that reducing GRK2 levels in myeloid cells, by attenuating pro-inflammatory features of macrophages, has a relevant impact in adipose-liver crosstalk, thus preventing high fat diet-induced metabolic alterations.

Keywords Obesity · Macrophages · GRK2 · Liver · Adipose tissue · Glucose homeostasis

Abbreviations

BMDM	Bone marrow-derived macrophages
CM	Conditioned media
COX-2	Cyclooxygenase-2
FA	Fatty acids
GRK2	G protein-coupled receptor kinase 2
GTT	Glucose tolerance test
HFD	High fat diet
HO-1	Heme oxygenase-1
iNOS	Inducible nitric oxide synthase
IR	Insulin resistance

Electronic supplementary material The online version of this article (https://doi.org/10.1007/s00018-019-03442-5) contains supplementary material, which is available to authorized users.

✉ Federico Mayor Jr
fmayor@cbm.csic.es

✉ Cristina Murga
cristina.murga@uam.es

1 Departamento de ciencias básicas de la salud, área de Bioquímica y Biología Molecular, Universidad Rey Juan Carlos (URJC), Madrid, Spain

2 Departamento de Biología Molecular and Centro de Biología Molecular "Severo Ochoa", Universidad Autónoma de Madrid (CSIC/UAM), C/Nicolás Cabrera 1, 28049 Madrid, Spain

3 Instituto de Investigación Sanitaria La Princesa, Madrid, Spain

4 CIBER de Enfermedades Cardiovasculares, Instituto de Salud Carlos III (ISCIII), Madrid, Spain

5 Laboratory of Translational Immunology (LTI), University Medical Center Utrecht, Utrecht University, Utrecht, The Netherlands

6 Instituto de Investigaciones Biomédicas Alberto Sols (CSIC-UAM), Madrid, Spain

7 CIBER de la Obesidad y la Nutrición (CIBEROBN), Instituto de Salud Carlos III (ISCIII), Madrid, Spain

8 Instituto de Investigación Biomédica de Málaga (IBIMA), Unidad de Endocrinología y Nutrición, Hospital Universitario Virgen de Victoria de Malaga, Universidad de Málaga, Málaga, Spain

9 University of Texas MD Anderson Cancer Center, Houston, TX, USA

ITT	Insulin tolerance test
LPS	Lipopolysaccharide
NAFLD	Non-alcoholic fatty liver disease
NASH	Non-alcoholic steatohepatitis
PTT	Pyruvate tolerance test
TEPMs	Thioglycollate -elicited peritoneal macrophages
TG	Triglycerides
TLR	Toll-like receptor
WAT	White adipose tissue

Introduction

Obesity is a key pathogenic factor associated with development of several metabolic alterations including non-alcoholic fatty liver disease (NAFLD), an extremely prevalent chronic liver disease worldwide, affecting about one quarter of adults in the developed countries [1]. Chronic nutrient excess results in the expansion and remodeling of adipose tissue, leading to unresolved inflammation, which is a major contributor to obesity-associated metabolic complications [2]. While acute inflammation at the early stage may work as an adaptive response, when obesity-associated inflammation becomes persistent, it finally triggers the so-called status of low-grade chronic inflammation. White adipose tissue (WAT) is mainly composed of adipocytes, immune cells and endothelial cells. Macrophages are the most abundant cell type among adipose-resident immune cells and are generally considered as the effector cells in the obesity-associated inflammation that contribute to insulin resistance (IR) [3]. Macrophages within adipose tissue of lean individuals are mainly M2 or alternatively activated macrophages, with a key role in maintaining tissue homeostasis through phagocytosis of dead adipocytes and secretion of anti-inflammatory cytokines and other regulatory factors [4]. However, obesity leads to a phenotypic switch from the anti-inflammatory M2 towards pro-inflammatory M1 macrophages, with upregulation of inflammatory markers (i.e. inducible nitric oxide synthase (iNOS), also known as NOS2) and production of factors that exacerbate inflammation [4, 5]. Macrophages in the M1 state signal for further macrophage recruitment, leading to a self-fed cycle of inflammation resulting in increased cytokine and fatty acid (FA) production. This finally interferes with insulin signaling and helps establish a global state of glycemic deregulation [6]. A similar situation has also been suggested for Kupffer cells, with the polarized response of these cells affecting the metabolism and insulin sensitivity of hepatocytes with implications for NAFLD and IR [7]. In addition, there is a close link between dysfunctional adipose tissue and NAFLD, and the crosstalk between dysfunctional adipocytes and the liver also involves macrophages that in concert promote the development of lipotoxic liver disease [8–10]. Therefore, the changes occurring in adipose tissue macrophages are important components of the etiology of IR [11] by amplifying inflammatory circuits in different tissues [12].

High fat diet (HFD) feeding, widely used as an experimental model of obesity in rodents, is known to trigger a state of low grade inflammation with increased pro-inflammatory macrophage infiltration in adipose tissue, a situation also observed in genetically obese mice and obese humans [13]. The Toll-like receptor (TLR) pathway has been suggested to drive low-grade inflammation in obesity-related metabolic diseases. Metabolic alterations associated to obesity or a HFD may change the composition of gut microbiota (dysbiosis), increasing gut barrier permeability, this allowing subsequent translocation of bacteria or bacterial products, including gram-negative bacterial cell wall components, namely lipopolysaccharide (LPS), the classical ligand for TLR4. Plasma LPS levels have been shown to be increased in obesity in animal models and humans. Such increase, defined as metabolic endotoxemia, has been shown to trigger low grade inflammation and metabolic disorders associated with obesity and type 2 diabetes [14–17]. In addition, during obesity high amounts of fatty acids (FA), which can activate TLR4, are released into the bloodstream [18]. Moreover, TLR4 has been reported to be upregulated in macrophages during obesity [6, 19] and its role in HFD-induced IR has been demonstrated in TLR4 whole-body knockout, hematopoietic cell-specific knockout, and LPS-resistant mice [20].

G protein-coupled receptor kinase 2 (GRK2) is a serine/threonine kinase classically known for its participation in the desensitization of multiple G protein-coupled receptors (GPCRs) together with arrestins [21]. However, emerging evidence has revealed that GRK2 interacts with a variety of proteins involved in signal transduction [22–24], and plays a relevant integrative role in the modulation of insulin response and metabolic homeostasis [25–27]. Interestingly, GRK2 is highly expressed in different cell types of the immune system. The levels and activity of this kinase are tightly regulated in immune cells [28, 29]. Moreover, inflammatory mediators regulate GRK2 levels [30] and leukocyte GRK2 is reduced in a number of inflammatory pathologies in mice and humans, including multiple sclerosis and rheumatoid arthritis (see [31] for a review). This suggests GRK2 as an important regulator of cell responses during inflammation with a potential role for this kinase in the onset or development of inflammatory disorders.

Given the key role of macrophages in obesity-related inflammatory processes and in tissue crosstalk in these contexts, we hypothesized that changes in GRK2 levels in this cell type may alter their inflammatory pattern and thus impact the development of diet-induced metabolic alterations in different tissues. Using a mouse model with

myeloid-lineage-specific GRK2 downregulation, we show here that decreasing GRK2 levels in myeloid cells diminishes the pro-inflammatory profile of macrophages, leading to reduced obesity-induced adipose tissue inflammation and prevention of obesity-related steatosis and hepatic IR, finally preserving glucose homeostasis.

Materials and methods

Mice

All mice used were in a C57Bl/6 J genetic background. Cre-loxP-mediated gene targeting was used to specifically delete GRK2 in cells from myeloid origin [32, 33]. Floxed homozygous GRK2 mice ($GRK2^{fl/fl}$) [34] and transgenic mice overexpressing a nuclear-localized Cre recombinase inserted into the first coding ATG of the lysozyme 2 gene (Lyz2) [B6.129P2-Lyz2tm1(cre)Ifo/J], obtained from the Jackson Laboratories, were mated. $GRK2^{f/f}$ LysM-$Cre^{-/-}$ controls (referred to as LysM-$GRK2^{+/+}$) and $GRK2^{f/\Delta}$ LysM-$Cre^{+/-}$ (referred to as LysM-$GRK2^{+/-}$) offspring were used. For some experiments, LysM-$GRK2^{+/-}$ offspring were backcrossed with $GRK2^{fl/fl}$ mice to obtain mice carrying both GRK2 alleles floxed as well as the LysM-Cre recombinase $GRK2^{\Delta/\Delta}$LysM-$Cre^{+/-}$ (referred to as LysM-$GRK2^{-/-}$). Animals were genotyped by PCR on genomic DNA using reported oligonucleotides [34].

Animal protocols

Mice were housed on a 12-hour light/dark cycle, at a temperature of 22 ± 2 °C with a relative humidity of $50 \pm 10\%$ and under pathogen-free conditions, with free access to food and water in the animal facility of the Centro de Biología Molecular Severo Ochoa (Madrid, Spain). At 8 weeks of age, mice were continued on a standard diet (SD) (2018S Harlan-Teklad, 12% calories from fat) or were fed a HFD (Envigo–formerly Harlan-, TD.07011, 54.4% calories from fat) during 12 weeks. At this point, glucose tolerance tests (GTTs), pyruvate tolerance tests (PTTs) and insulin tolerance tests (ITTs) were performed. Body weight was measured weekly. Before sacrifice, some mice were intraperitoneally injected with either vehicle or insulin (Actrapid®, Novo Nordisk, 1 IU/Kg body weight). After 10 min, mice were euthanized, tissues were surgically removed, immediately weighted and either fixed or frozen in liquid nitrogen to be stored at −80 °C. All animal experimentation procedures conformed to the European Guidelines for the Care and Use of Laboratory Animals (Directive 86/609) and were approved by the Ethical Committees for Animal Experimentation of our Institutions and the Comunidad de Madrid.

Metabolic assays

GTTs and ITTs were performed as previously described [35]. Glucose (2 g/Kg body weight), and insulin (0.8 U/kg body weight) were administered intraperitoneally. For the PTT, after an overnight fasting, mice received an intraperitoneal injection of 1.5 g/kg sodium pyruvate (Merck) dissolved in 0.9% NaCl [36]. For the LPS- induced glucose intolerance, 1 mg/kg of body weight of LPS (Sigma-Aldrich) dissolved in 0.9% NaCl was injected intraperitoneally 48 h prior to glucose determinations. Glucose concentration was determined in tail blood samples using an automatic analyzer (One Touch Ultra, LifeScan). Serum insulin concentration was measured by ELISA (Mercodia) and circulating non-esterified fatty acids (NEFA) by an enzymatic method (NEFA-HR kit Wako Chemicals).

Adipocyte size determination

Adipose tissue sections were stained with haematoxylin and eosin for the evaluation of adipocyte size. Individual adipocyte areas within each field were determined using image analysis software (ImageJ). Adipocyte size was calculated in arbitrary fields by quantitation of 150 cells in at least four different randomly chosen fields per mouse.

Immunohistochemical detection of the F4/80 macrophage marker

Liver tissue sections were de-paraffinized and rehydrated, and slides were incubated overnight with the primary antibody anti-F4/80 (clone BM8, Abcam) to perform immunohistochemical detection as described [35]. A negative control in the absence of the primary antibody was used. The presence of macrophages (positive area in F4/80 stained sections) was determined using image analysis software (ImageJ). Three to five different high-power fields from each section were analyzed per animal.

Liver triglyceride content determination

A piece of approximately 50 mg of frozen tissue was lysed in 1 ml of isopropyl alcohol using Tissue Lyser (Qiagen) metal beads for 2 pulses of 1 min each at 30 Hz and centrifuged at 2000 g for 10 min at 4 °C. The amount of triglycerides (TG) in the supernatant was measured using an enzymatic method with the Serum Triglyceride Determination Kit (TR0100, Sigma-Aldrich).

Microbiota analysis

Fecal samples were collected and immediately stored at − 80 °C until analysis. DNA extraction from stools was performed using the QIAamp DNA stool Mini kit (Qiagen, Hilden, Germany) according to the manufacturer's instructions. DNA concentrations were determined by absorbance at 260 nm (A260). Purity was estimated by determining the A260/A280 ratio. Both measurements were performed with a Nanodrop spectrophotometer (Nanodrop Technologies).

Ribosomal 16S rRNA gene sequences were amplified from DNA using the 16S Metagenomics Kit (Thermo Fisher Scientific, Italy). The kit included two primer sets that selectively amplify the corresponding hypervariable regions of the 16S region in bacteria: primer set V2–4–8 and primer set V3–6, 7–9. Libraries were created using the Ion Plus Fragment Library Kit (Thermo Fisher Scientific). Barcodes were added to each sample using the Ion Xpress Barcode Adapters kit (Thermo Fisher Scientific). Emulsion PCR and sequencing of the amplicon libraries was performed on an Ion 520 chip (Ion 520TM Chip Kit) using the Ion Torrent S5TM system and the Ion 520TM/530TM Kit-Chef (Thermo Fisher Scientific) according to the manufacturer´s instructions. After sequencing, the individual sequence reads were filtered using Ion Reporter Software V4.0 to remove low quality and polyclonal sequences.

Sequences were further translated into amplicon sequence variants (ASVs) using DADA2 with adapted parameters for Ion Torrent data [37] within the microbiome analysis package QIIME2 (www.qiime2.org) [38], which was also used for diversity analysis and subsequent taxonomic analysis through clustering with vsearch [39] and the reference base Greengenes version 13_8 at 97% of identity. Further differential abundance analysis was assessed with ANCOM [40].

Flow cytometry analysis

Epididymal adipose tissue (eWAT) was isolated, washed with PBS and minced into small pieces with scissors. Tissue was digested with type II collagenase (Sigma-Aldrich) at 37ºC for 1 h with vigorous shaking. After digestion, cell suspension was filtered through a 100 µm nylon filter and centrifuged at 500 g to pellet the cells from the stromal vascular fraction (SVF). Pellet was suspended in FACS buffer (PBS 1x, 1% BSA, 1% FCS) to a concentration of 0.3 to 0.5×10^6 cells in 100 µl. Cell suspension was incubated for 10 min with 0.5 µl of Fc-block (anti CD16/32) and then with the different primary antibodies (F4/80-FITC, CD11b-APC, CD11c-PE, from eBiosciences) protected from light for 30 min. Pooled samples were used for the single stained (SS) and florescence minus-one (FMO) controls. Cell viability was tested with DAPI. FACSCanto II from Beckton and Dickinson was used for the analysis of the samples.

Cell culture

Experiments on thioglycollate-elicited macrophages Macrophages were recruited to the peritoneal cavity by thioglycollate injection, as previously described [41]. Thioglycollate-elicited peritoneal macrophages (TEPM) were isolated from 12–16-week-old LysM-GRK2$^{+/+}$ and LysM-GRK2$^{+/-}$ male mice by peritoneal lavage 5 days post-i.p. injection with thioglycollate (Difco Laboratories). Macrophages were centrifuged for 5 min at 300 g, cultured at 2×10^6/well in 6-well flat-bottomed plates in RPMI-1640 medium supplemented with 10% FBS and purified by adherence to tissue culture plates for 2 h. 24 h after isolation macrophages were serum-starved overnight, and subsequently incubated or not with 1µg/ml lipopolysaccharide (LPS) (Sigma-Aldrich) for 6 h. Supernatants were harvested for further experiments. The GRK2/3-specific inhibitor Cmpd101 (30 µM; Hello Bio) was added 20 min before LPS treatment when specified.

Differentiation and treatment of 3T3L1 preadipocytes 3T3L1 preadipocytes were cultured in DMEM supplemented with 10% FBS and differentiated as previously described [42]. At day 10 post-differentiation, adipocytes were serum starved (1% FBS) overnight and further incubated with the conditioned medium of macrophages from LysM-GRK2$^{+/+}$ or LysM-GRK2$^{+/-}$ treated or not with 1µg/ml LPS. 24 h later, 3T3L1 adipocytes were stimulated with insulin at 10 nM for 10 min before lysis.

Isolation, differentiation and treatment of bone marrow-derived macrophages (BMDM) Total bone marrow was obtained by flushing femurs and tibias from 10–12 weeks old C57BL/6 J mice with DMEM containing 10%FBS (Gibco 41,966,029). Bone marrow mononuclear phagocytic precursor cells were propagated in suspension by culturing in DMEM containing 10% FBS, 100 U/ml penicillin, 100 µg/ml streptomycin and 20 ng/ml recombinant murine M-CSF (PeproTech 315–02). The precursor cells became adherent within 7 days of culture. Cells were then harvested and seeded in 12 multi-well culture plates (10^6 cells per well) in complete medium. Next day, cells were washed with PBS and treated with the corresponding conditioned medium for 24 h. Finally, medium was collected for nitrite determination and plates were stored at -80ºC until processing.

Nitrite determination

Nitric oxide release was determined from the amount of accumulated nitrites in cell supernatants, measured spectrophotometrically according the Griess reaction. The absorbance at 542 nm was compared with a $NaNO_2$ standard.

Western Blot analysis

Tissues were homogenized using metal beads in a Tissue Lyser and cells were lysed in hypotonic lysis buffer as previously described [36]. 30–50 µg of total protein was resolved per lane by SDS-PAGE and transferred to a nitrocellulose membrane.

Blots were probed with specific antibodies against cyclooxygenase-2 (COX-2) and heme oxygenase-1 (HO-1) (Millipore), iNOS, and (GRK2) (Santa Cruz), phospho (Ser473) and total AKT (Cell Signaling) β-actin and GAPDH (Sigma) as previously described [43]. Immunoreactive bands were visualized using enhanced chemiluminescence (ECL; Amersham Biosciences) or the Odyssey Infrared Imaging System (Li-Cor Biosciences). Films were scanned with a GS-700 Imaging Densitometer and analyzed with Quantity One Software (Bio-Rad), or using an Odyssey Classic reader and the Odyssey software package 3.0 (Li-Cor Biosciences).

mRNA isolation and Real Time PCR

RNA was extracted using metal beads in a Tissue Lyser and the RNeasy Mini Kit (Qiagen) following the instructions provided by the supplier. Quantity and quality of RNA were analyzed using Nanodrop ND-1000 (Thermo Scientific).

RT-PCRs were performed in the Genomic Facility at CBMSO using Light Cycler equipment (Roche) and self-designed probes purchased from Sigma with Syber Green technology. Primers used are shown in Supplementary Table 1. A geometric mean of three stably expressed and commonly used reference genes (*Ywhaz*, *Gapdh* for the liver; *B2m*, *Ppia* for eWAT) was used for data normalization. qPCRs and statistical analysis of the data were performed using GenEx software.

Multiplex analysis of cytokines

Experimental supernatants from LPS-treated TEPMs were collected and centrifuged at 3,000 g for 5 min. Cytokine concentration was determined for TNF-α, IL-6 and IL-10, using an ELISA kit purchased from R&D systems. Supernatants were analyzed in duplicates using the manufacturer's protocol.

Data analysis

All data are expressed as mean values ± SEM and n represents the number of animals. Statistical significance was analyzed by using unpaired Student's *t* test or Mann-Withney test depending on the distribution of the data, or one- or two-way ANOVA followed by Bonferroni's *post-hoc* test, or Kruskal–Wallis test followed by Dunns *post-hoc* test when the distribution of the samples was not normal. Differences were considered statistically significant when P value < 0.05.

Results

Myeloid cell-specific decrease in GRK2 levels protects against HFD-induced glucose intolerance

To evaluate the role of GRK2 in the crosstalk between myeloid cells and other tissues during the development of obesity-induced IR, LysM-GRK2$^{+/+}$ control mice, as well as LysM-GRK2$^{+/-}$ and LysM-GRK2$^{-/-}$ littermates, were either fed a standard diet (SD) or a HFD for 12 weeks. As shown in Fig. 1a, both LysM-GRK2$^{+/-}$ and LysM-GRK2$^{-/-}$ mice were protected against HFD-induced hyperglycemia while they did not develop hyperinsulinemia, but rather presented decreased fasting insulin levels compared with LysM-GRK2$^{+/+}$ littermates after the HFD (Fig. 1b). Accordingly, LysM-GRK2$^{+/-}$ and LysM-GRK2$^{-/-}$ mice showed improved glucose homeostasis in the glucose tolerance test (GTT) after the HFD without differences among genotypes on SD (Fig. 1c, d). Indeed, the area under the curve (AUC) showed a significant enhancement of glucose tolerance in LysM-GRK2$^{+/-}$ and LysM-GRK2$^{-/-}$ mice at the end of the HFD feeding period (Fig. 1e) that was more evident when the levels of GRK2 were lower as in the LysM-GRK2$^{-/-}$ group.

The amelioration of glucose tolerance in LysM-GRK2$^{+/-}$ mice occurs in the absence of important differences in systemic insulin sensitivity or body weight gain

Despite the improvement in glucose tolerance observed in LysM-GRK2$^{+/-}$ and LysM-GRK2$^{-/-}$ mice on HFD, no significant differences were found in the insulin tolerance test (ITT) among genotypes on either SD or HFD, except for a slight improvement at 60 min in LysM-GRK2$^{-/-}$ HFD-fed mice (Fig. 2a,b) that did not reach significance when the AUC was analyzed (Fig. 2c). Since muscle accounts for an important percentage of insulin-induced glucose clearance, these data suggested that the protection against HFD-induced glucose intolerance observed in LysM-GRK2$^{+/-}$ and LysM-GRK2$^{-/-}$ mice might not be due to important differences

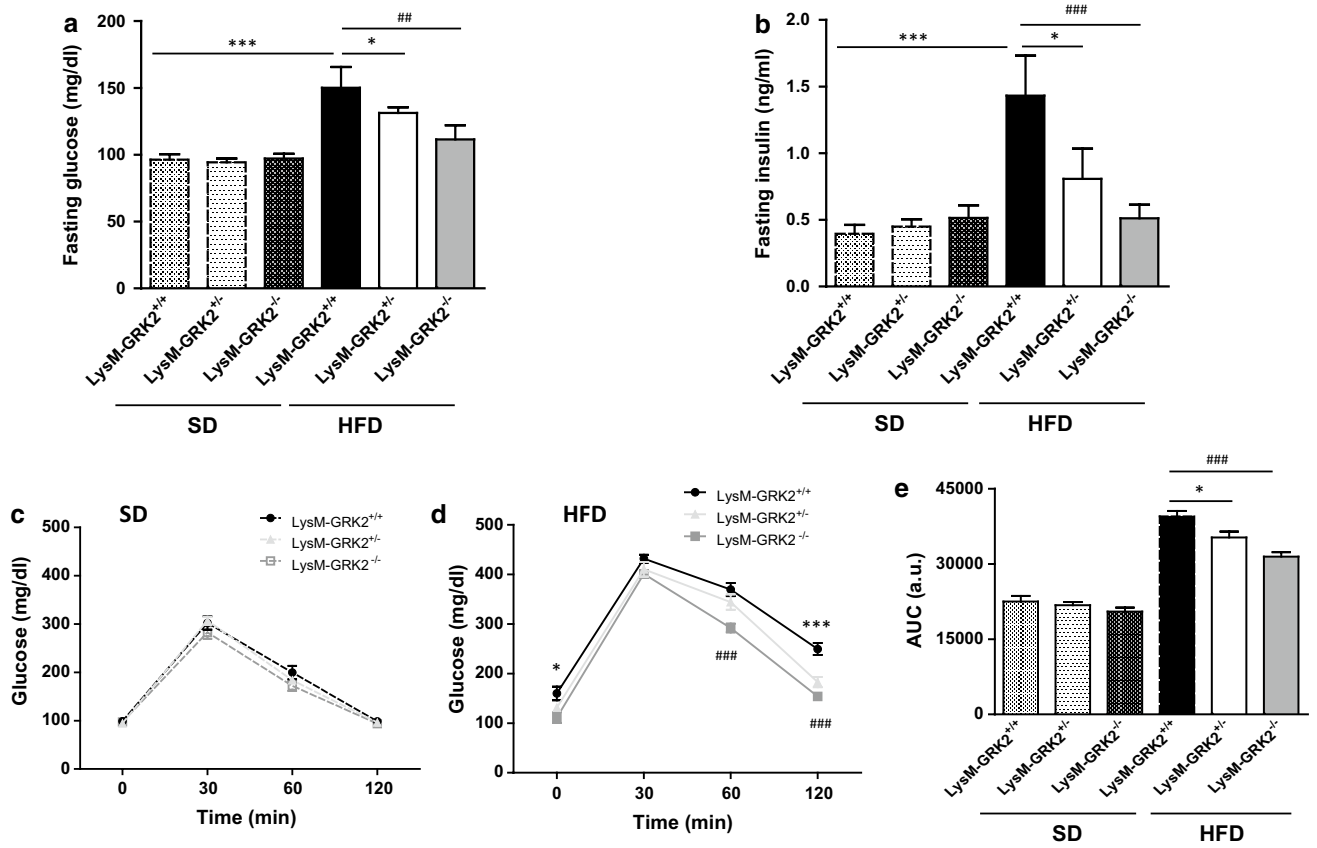

Fig. 1 Decreasing GRK2 levels in myeloid cells protects against the development of HFD-induced glucose intolerance. 8-week old male mice from the LysM-GRK2$^{+/+}$, LysM-GRK2$^{+/-}$ or LysM-GRK2$^{-/-}$ genotypes were either maintained on a SD or fed a HFD for 12 weeks. At the end of this period, serum glucose (**a**) and insulin (**b**) levels were measured upon an overnight fasting (~12 h). Intraperitoneal GTTs in the SD-fed (**c**) and the HFD-fed (**d**) groups were performed. **e** Histogram showing the GTTs area under the curve (AUC) analysis. Results are means ± SEM of 5–8 animals per group. Statistical analysis was performed by one-way (**a** and **b**) or two-way (**e**) ANOVA or by two-way repeated measures ANOVA (c and d) followed by Bonferroni's *post-hoc* test. ($^{*}p<0.05$; $^{**}p<0.01$; $^{***}p<0.005$ and $^{\#\#}p<0.01$; $^{\#\#\#}p<0.005$ for LysM-GRK2$^{+/+}$ *vs* LysM-GRK2$^{-/-}$ comparison)

in muscle insulin sensitivity. Furthermore, the percentage of body weight gain did not differ between groups in the SD-fed mice (Fig. 2d) and no significant differences were found between LysM-GRK2$^{+/+}$ and LysM-GRK2$^{+/-}$ during the 12 weeks of HFD (Fig. 2e, f). In HFD-fed LysM-GRK2$^{-/-}$ mice, however, we found a decreased body weight gain. So, we cannot rule out the contribution of the leaner phenotype to the improved glucose homeostasis detected in these mice.

Low levels of GRK2 in myeloid cells protect mice from HFD-induced increase in hepatic glucose production

In order to evaluate hepatic regulation of glucose homeostasis in our model, we performed a pyruvate tolerance test. Pyruvate administration elicits a glycemic profile that reflects the status of hepatic gluconeogenesis, and that is increased in the insulin-resistant liver thus contributing to the characteristic hyperglycemia [44]. Lowering GRK2 levels in myeloid cells conferred protection against HFD-induced dysregulation in the control of gluconeogenesis to the same extent in LysM-GRK2$^{+/-}$ and LysM-GRK2$^{-/-}$ mice, without differences between genotypes in SD-fed mice (Fig. 2g–i).

Since LysM-GRK2$^{+/-}$ mice show a very similar phenotype to LysM-GRK2$^{-/-}$ animals regarding glucose homeostasis and systemic insulin sensitivity, we continued our study specifically the LysM-GRK2$^{+/-}$ mice. This decision was driven by the fact that body weight gain during a HFD strongly influences IR, so models in which body weight is comparable after the HFD might be considered advantageous if the aim is to specifically investigate the contribution of inflammation to HFD-induced metabolic alterations. Moreover, a partial decrease of GRK2 levels in macrophages rather than a complete deletion would reflect in a more physiological manner

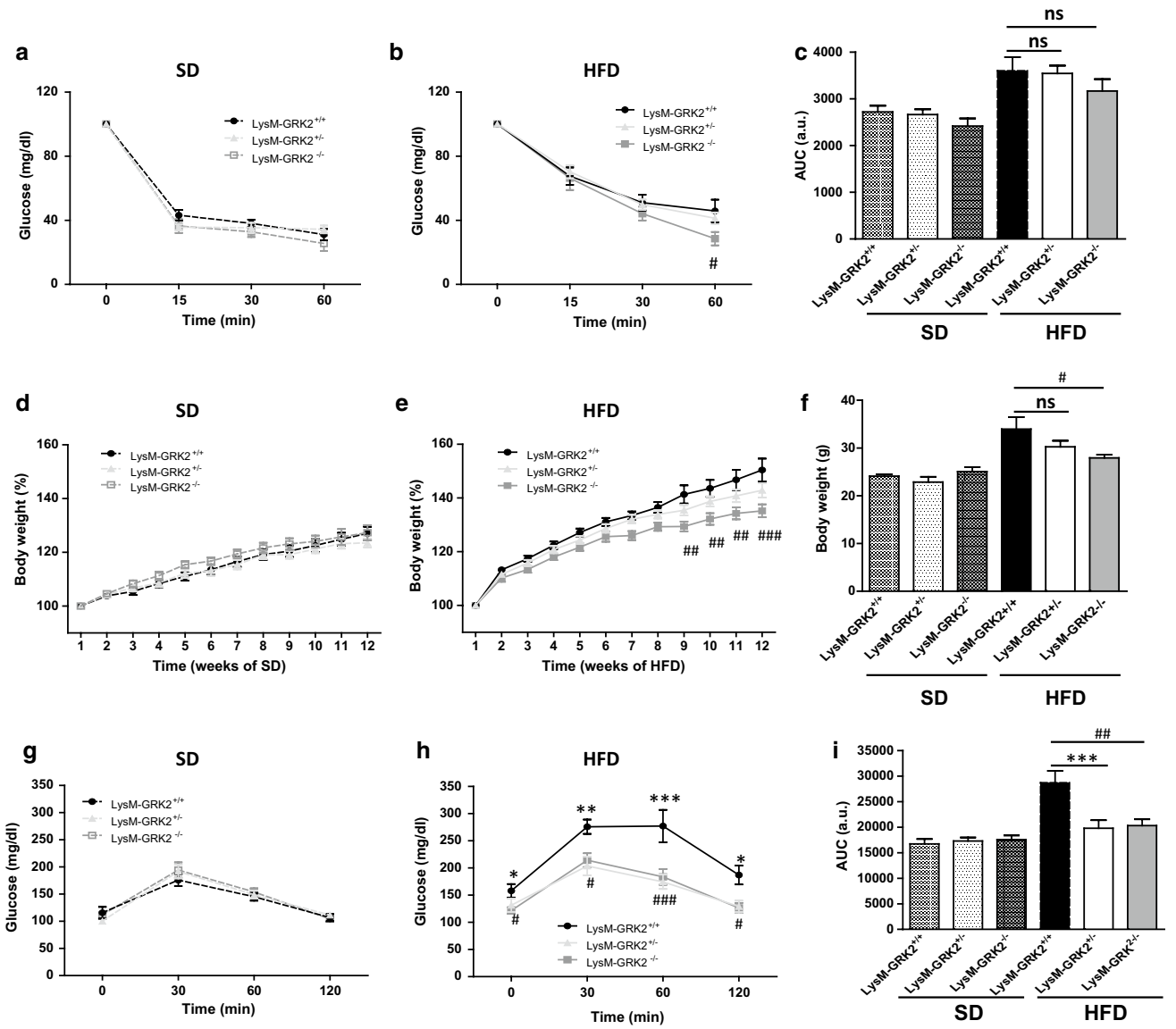

Fig. 2 Decreasing GRK2 levels in myeloid cells does not cause important differences in systemic insulin sensitivity or body weight gain, but significantly improves pyruvate tolerance in HFD-fed mice. 8-week old male mice from the LysM-GRK2$^{+/+}$, LysM-GRK2$^{+/-}$ or LysM-GRK2$^{-/-}$ genotypes were either maintained on a SD or fed a HFD for 12 weeks. Intraperitoneal ITTs in the SD-fed **a** and the HFD-fed **b** groups were performed. **c** Histogram showing the ITTs AUC analysis. Body weight evolution (expressed in %) during the 12 weeks of standard (**d**) or high fat (**e**) feeding, and final body weight at the end of the 12 weeks are shown (**f**). Intraperitoneal pyruvate tolerance tests (PTTs) in the SD-fed (**g**) and the HFD-fed (**h**) groups were performed. **i** Histogram showing the PTTs AUC analysis. Results are means ± SEM of 5–8 animals per group. Statistical analysis was performed by two-way repeated measures ANOVA followed by Bonferroni's *post-hoc* test. ($^{*}p<0.05$; $^{**}p<0.01$; $^{***}p<0.005$ and $^{\#}p<0.05$; $^{\#\#}p<0.01$; $^{\#\#\#}p<0.005$ for LysM-GRK2$^{+/+}$ *vs* LysM-GRK2$^{-/-}$ comparison)

what may occur in health and disease, and also represents a more faithful model to recapitulate the effect of a treatment with a pharmacological GRK2 inhibitor that would not completely block GRK2 actions. Thus, we decided to focus our study in mice with lower, but no completely absent, levels of GRK2 in myeloid cells (LysM-GRK2$^{+/-}$ mice).

Lower GRK2 levels in myeloid cells limits insulin resistance, inflammation and adipocyte hypertrophy in eWAT upon a HFD

During obesity, white adipose tissue (WAT) may become severely dysfunctional, leading to metabolic alterations and to activation of pro-inflammatory macrophages. In fact, the link between obesity, adipocyte hypertrophy, inflammation

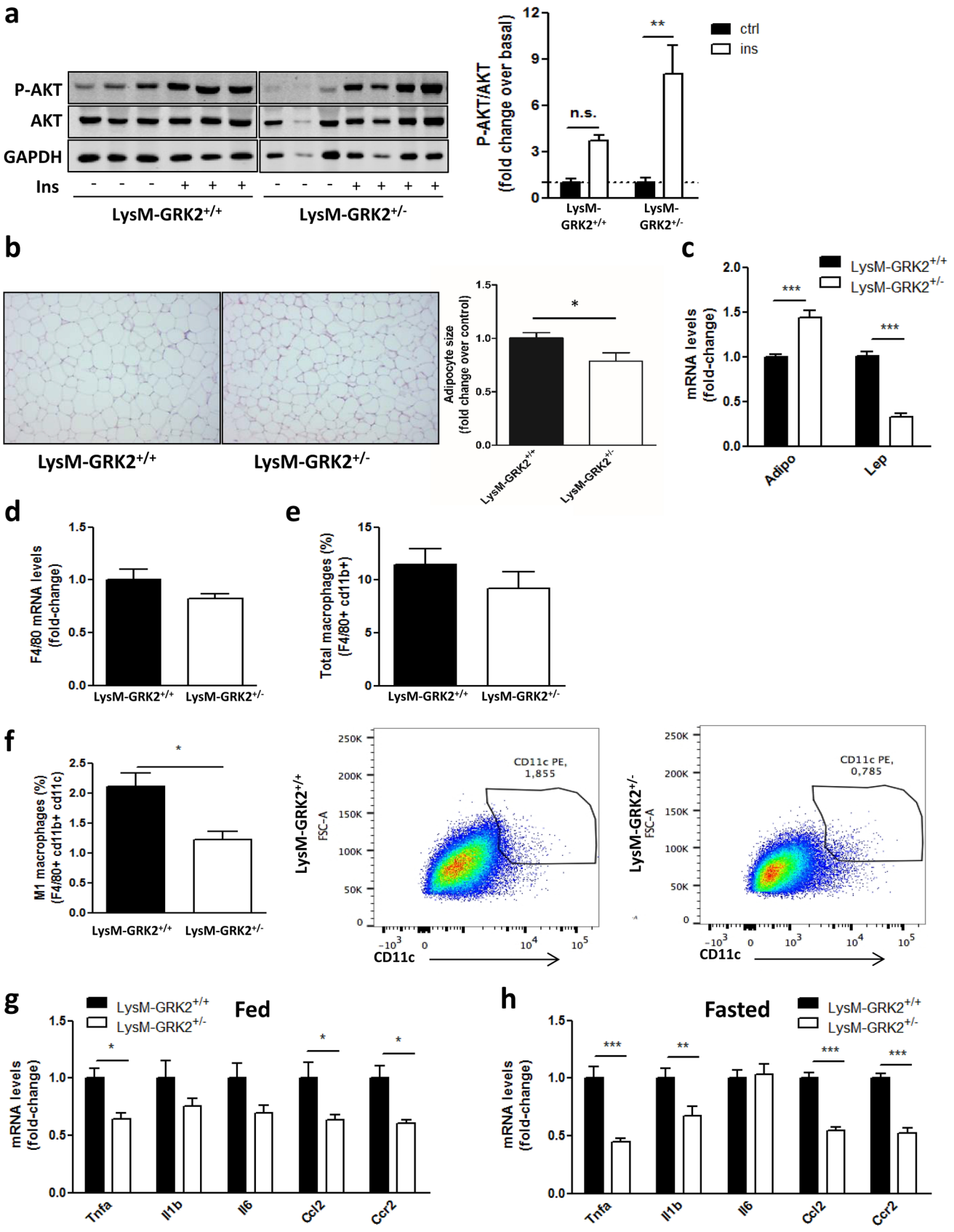
a
P-AKT
AKT
GAPDH
Ins
LysM-GRK2+/+
LysM-GRK2+/-
P-AKT/AKT (fold change over basal)
ctrl
ins
n.s.
**
b
Adipocyte size (fold change over control)
*
c
mRNA levels (fold-change)
***
Adipo
Lep
d
F4/80 mRNA levels (fold-change)
e
Total macrophages (%) (F4/80+ cd11b+)
f
M1 macrophages (%) (F4/80+ cd11b+ cd11c)
CD11c PE, 1,855
CD11c PE, 0,785
FSC-A
CD11c
g
Fed
Tnfa
Il1b
Il6
Ccl2
Ccr2
h
Fasted

◂**Fig. 3** HFD-fed LysM-GRK2$^{+/-}$ mice show increased insulin-induced AKT phosphorylation in eWAT, together with reduced adipocyte size and a less dysfunctional adipokine and cytokine expression profile upon a HFD. Following 12 weeks of HFD, control (LysM-GRK2$^{+/+}$) and LysM-GRK2$^{+/-}$ mice were injected vehicle (NaCl 0.9%) or insulin (1 IU/kg body weight) and after 10 min tissue lysates from eWAT were subjected to WB and probed with antibodies against total and phosphorylated AKT (Ser473). Representative immunoblots and densitometric analysis (**a**) of four mice per group are shown and expressed as % of stimulation over vehicle-injected mice (basal). Statistical significance was analyzed by unpaired two-tailed t test $*p < 0.05$. **b** Sections of epididymal fat pads from control and LysM-GRK2$^{+/-}$ mice stained with haematoxylin and eosin (10×magnification). Representative photomicrographs are shown. Adipocyte size was calculated by determining individual adipocyte areas using image analysis software (ImageJ) in 2–5 different randomly chosen fields per mouse, in 6–7 mice per genotype. Statistical significance was analyzed by unpaired two-tailed *t* test $*p < 0.05$. **f** Total macrophages in the adipose SVF were identified by FACS gating F4/80 and cd11b positive cells, and expressed as % from parental cells. **f** M1 macrophages were identified by flow cytometry, as depicted by representative images, as the CD11c-positive cells within the F4/80 and CD11b-positive cells, and expressed as % from parental cells. Data are represented as means ± SEM of 5–6 mice per genotype. eWAT lysates were subjected to real-time qPCR to measure the expression of *Adiponectin* and *Leptin* genes (**c**) *Emr1* (F4/80) gene (**d**) as well as the expression of genes encoding TNFα, IL-1β, IL-6, CCL-2 (MCP-1) and CCR2 in fed (**g**) or overnight fasted (~ 12 h) (**h**) mice. qPCR results were normalized against *Ppia* and *B2m* mRNAs. Statistical significance was analyzed by unpaired two-tailed t test (**c**) or by one-way ANOVA followed by Bonferroni *post-hoc* test (**f**, **g**) ($*p < 0.05$; $***p < 0.005$)

and IR is well known. At the molecular level, binding of insulin to its receptors in the cell surface causes subsequent phosphorylation of the downstream target AKT, and this phosphorylation is impaired in situations of IR. We found that insulin-induced AKT phosphorylation in WAT of LysM-GRK2$^{+/-}$ mice was significantly increased compared to LysM-GRK2$^{+/+}$ littermates despite the HFD feeding (Fig. 3a). This enhanced insulin sensitivity correlated with a decreased adipocyte size in LysM-GRK2$^{+/-}$ mice (Fig. 3b) and an increased expression of *Adiponectin* concomitant with a decreased expression of *Leptin* genes in adipose tissue from these animals (Fig. 3c). No differences were detected between genotypes in GRK2 levels in whole WAT lysates (Fig. S1).

Interestingly, the total number of macrophages in adipose tissue was not different between genotypes neither in terms of F4/80 mRNA levels (Fig. 3d) nor quantifying F4/80 cd11b-positive cells by FACS (Fig. 3e). Nevertheless, the percentage of M1 macrophages, as defined by CD11c expression, was clearly reduced in LysM-GRK2$^{+/-}$ mice (Fig. 3f). We also observed a significant reduction in the expression of the pro-inflammatory cytokine TNFα, the chemokine MCP-1 (CCL2) and of its receptor CCR2, together with an almost significant tendency towards decreased IL1β and IL-6 gene expression in WAT from HFD-fed LysM-GRK2$^{+/-}$ mice (Fig. 3g). Fasting is a stimulus known to activate adipose tissue lipolysis, increasing local levels of free fatty acids, which activate classical inflammatory responses in macrophages through engagement of pattern recognition receptors, including TLR4 [18]. Despite no differences were found in total circulating NEFA levels between genotypes (Fig. S2), the mRNA expression of inflammatory cytokines TNFα and IL1β as well as the mRNA of the chemokine MCP-1 and its receptor CCR2 were also decreased in adipose tissue from HFD-fed LysM-GRK2$^{+/-}$ mice upon a 12 h fasting (Fig. 3h). Since macrophages within adipose tissue are known to respond to obesity by a specific inflammatory program that further stimulates disease progression, our data suggested that the reduced inflammatory response of WAT macrophages with decreased GRK2 levels may contribute to the observed phenotype.

Insulin signaling is increased in the liver of HFD-fed LysM-GRK2$^{+/-}$ mice, together with decreased steatosis and inflammation

Adipose tissue macrophages in the visceral compartment not only promote local inflammation, but also contribute to systemic glycemic control and have an important role in the development of global and hepatic IR and in NAFLD severity [10]. We thus analyzed the activation of the insulin pathway in the liver as a key contributor to glucose homeostasis. In accordance to the profile observed in the GTT and the PTT (Figs. 1d–e; 2h–i) and with data obtained in WAT (Fig. 3a), LysM-GRK2$^{+/-}$ mice displayed an improved hepatic insulin response, since insulin-induced AKT phosphorylation was preserved in the liver of HFD-fed LysM-GRK2$^{+/-}$ animals compared to control littermates (Fig. 4a).

Because IR favors the accumulation of excessive hepatic fat, we performed a histological analysis and observed a marked steatosis in livers of HFD-fed control mice but not of LysM-GRK2$^{+/-}$ animals (Fig. 4b). Coherently, the TG content of the liver was significantly lower in HFD-fed LysM-GRK2$^{+/-}$ mice (Fig. 4c). Closely linked to both, hepatic steatosis and IR, the activation of liver-resident Kupffer cells helps recruit blood-derived monocytes. Both differentiate into pro-inflammatory macrophages and further promote NAFLD progression [10]. Therefore, the presence of hepatic macrophages was assessed by immunostaining (Fig. 4d) and mRNA expression analysis (Fig. 4e) for F4/80, a macrophage and Kupffer cell marker. We found reduced F4/80 protein and mRNA levels in the liver of HFD-fed LysM-GRK2$^{+/-}$ mice, suggesting a decreased presence of macrophages in the liver of these animals, together with a decreased expression of mRNAs of the pro-inflammatory cytokines TNFα, IL1β and IL6 or for CCL2 and CCR2 (Fig. 4f), known to contribute to hepatic IR in obesity [45]. Moreover, *Ptgs2* mRNA was also reduced in the liver of mice with lower levels of GRK2 (Fig. 4g), what is consistent

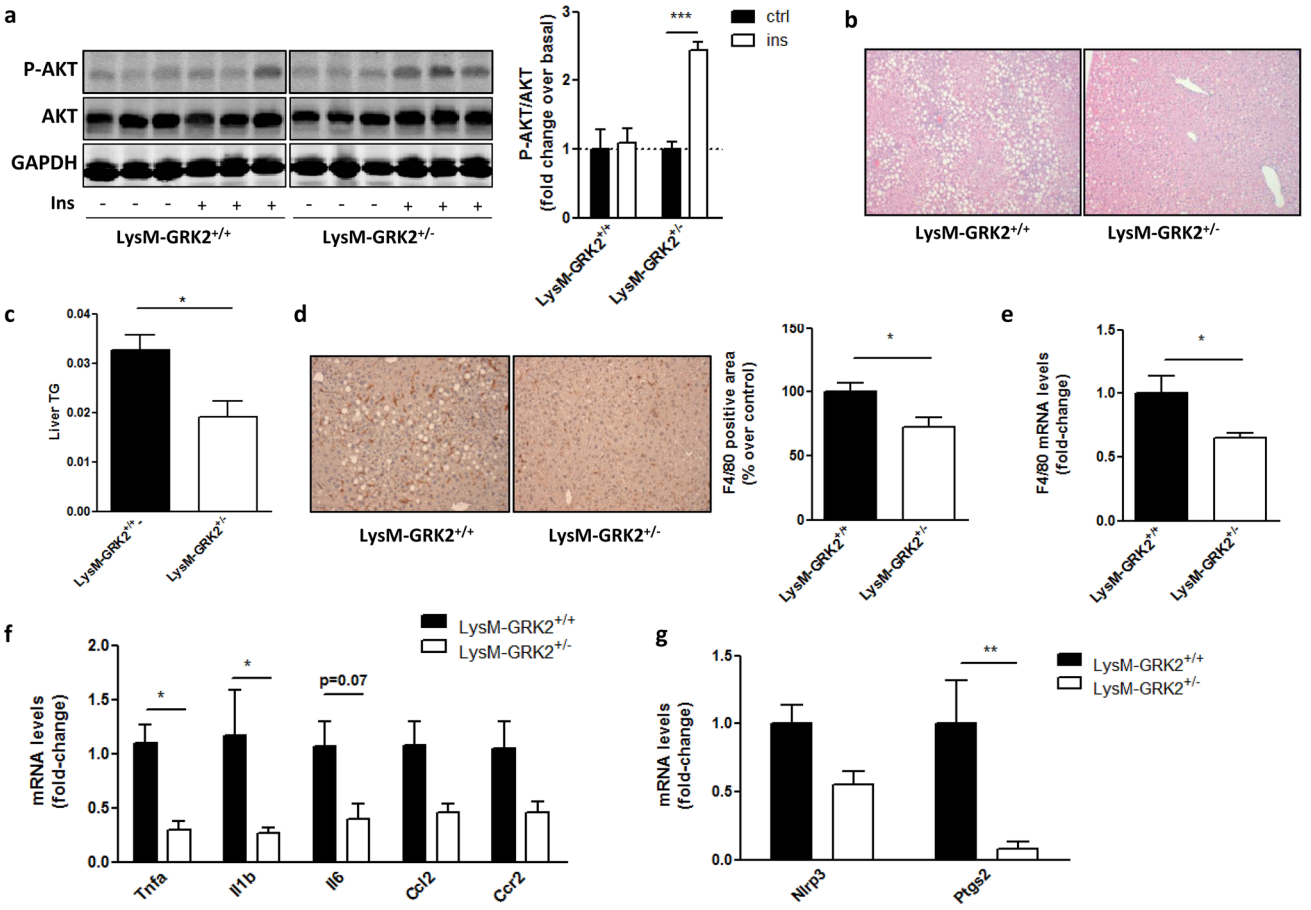

Fig. 4 Insulin signaling is increased in the liver of HFD-fed LysM-GRK2$^{+/-}$ mice, accompanied by decreased steatosis and inflammation. Following 12 weeks of HFD, control (LysM-GRK2$^{+/+}$) and LysM-GRK2$^{+/-}$ mice were injected vehicle (NaCl 0.9%) or insulin (1 IU/kg body weight) and after 10 min tissue lysates from liver were subjected to western blot (WB) and probed with antibodies against total and phosphorylated AKT (Ser473). Representative immunoblots and densitometric analysis (**a**) of four mice per group are shown. Results are expressed as % of stimulation over vehicle-treated mice (basal). **b** Liver sections from HFD-fed mice from both genotypes were stained with haematoxylin and eosin (10×magnification). **c** Liver TG were extracted, measured and expressed as equivalent triolein concentration (mg/ml). Data are means±SEM of 6 animals per genotype. Statistical significance was analyzed by unpaired two-tailed *t* test *$p < 0.05$ **d** Immunohistochemical analysis of liver sections stained with F4/80 antibody and counterstained with haematoxylin (magnification×20). Representative photomicrographs are shown. Positively stained area was quantified using Image J Software in at least three different randomly chosen fields per mouse. Results are expressed as % change over control (HFD-fed LysM-GRK2$^{+/+}$) mice and are means ± SEM of 6 animals per genotype. Statistical significance was analyzed by Mann Whitney test *$p < 0.05$. Real-time quantitative polymerase chain reaction (qPCR) was used to measure the hepatic expression of the F4/80 gene (**e**) and genes encoding TNF- , IL-1beta, IL-6, CCL2, CCR2 (**f**) and NRLP3 and COX-2 (*Ptgs2*) (**g**). Results were normalized against *Ywhaz* and *Gapdh* mRNAs. Values are represented as fold change over control mice and are means ± SEM of 5–6 animals per genotype. Statistical significance was analyzed by unpaired two-tailed *t* test (**e**) or by one-way ANOVA followed by Bonferroni *post-hoc* test (**f**, **g**) (*$p < 0.05$; **$p < 0.05$)

with its expression being mediated by TNFα and IL1β, and the expression of *Nlrp3* inflammasome, which plays a key role in the processing of bioactive IL1β and has been involved in the progression of NAFLD to non-alcoholic steatohepatitis (NASH) [46], showed a trend towards a decreased expression. These results suggest that reducing GRK2 levels specifically in myeloid cells has substantial consequences in the development of IR and inflammation in the liver, and highlight an important role for myeloid GRK2 in the regulation of the interplay between macrophages, adipocytes and hepatocytes in HFD-induced conditions.

Differences in microbiota do not play a major role in the protection against glucose intolerance conferred by decreased GRK2 levels in myeloid cells

Besides saturated fatty acids, another driver of pro-inflammatory macrophage activation within WAT is microbiota-derived LPS [47]. Since changes in gut microbiota composition have been commonly observed during a HFD feeding [16, 48] and contribute to the phenotype, we evaluated the potential contribution of microbiota alterations in the protection observed in LysM-GRK2$^{+/-}$ mice. No significant

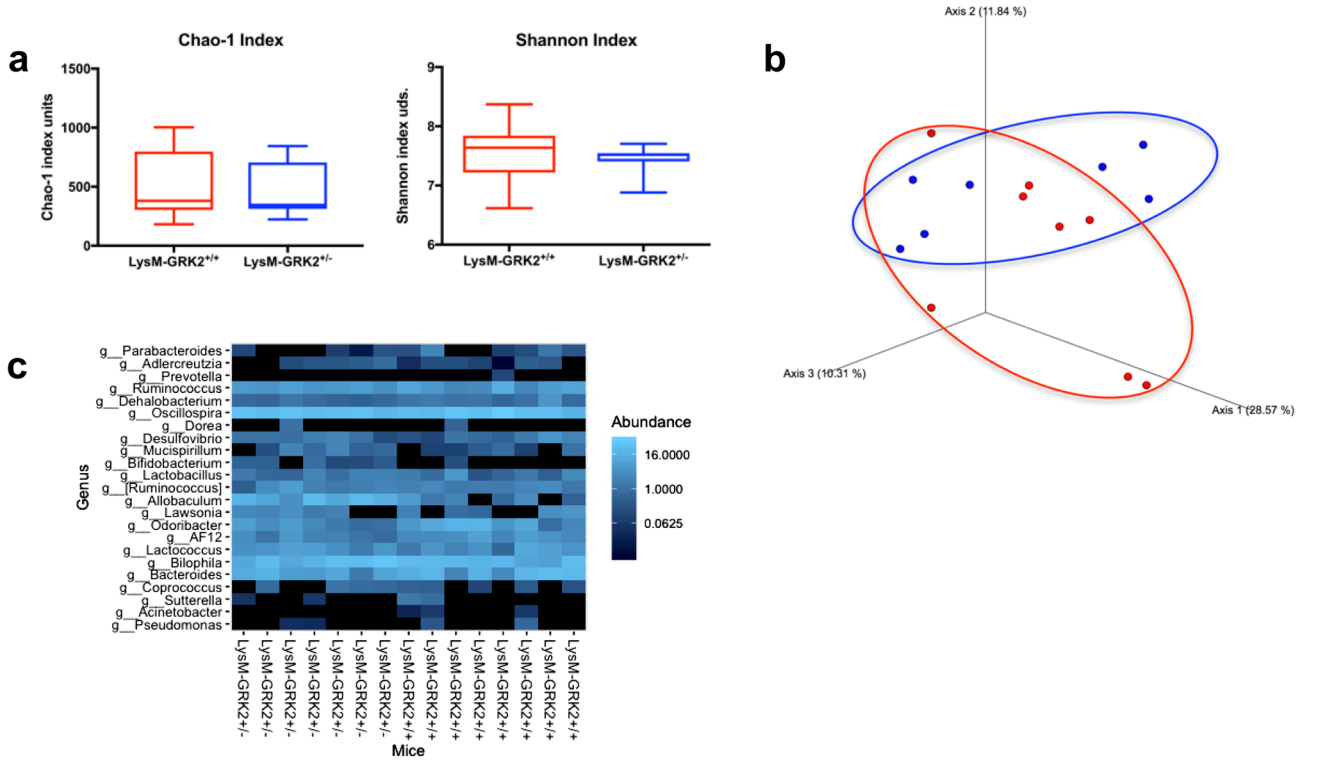

Fig. 5 Gut microbiota analysis from LysM-GRK2$^{+/+}$ and LysM-GRK2$^{+/-}$ mice under a HFD. **a** Comparison of Chao1 and Shannon diversity indexes between groups. Statistical differences were analyzed by Kruskal Wallis test. No differences were observed. **b** Principal coordinates analysis (PCoA) plot of Unweighted Unifrac distance of fecal samples collected after 12w from LysM-GRK2$^{+/+}$ and LysM-GRK2$^{+/-}$ mice fed a HFD. PERMANOVA analysis did not show statistical differences between groups. **c** Heatmap for the effect of genetics on intestinal microbiota composition showing bacterial groups at genus level. Relative abundances of the groups are color-coded from less to more abundance

differences were found in Chao1 or Shannon diversity indexes (Fig. 5a) nor in their whole populations as measured through the Unweighted Unifrac distance of fecal samples collected from control and LysM-GRK2$^{+/-}$ mice after 12 weeks of HFD (Fig. 5b). Accordingly, the heatmap showing relative abundances of bacterial groups at the genus level does not show significant differences between groups upon 12 weeks of HFD (Fig. 5c). It should be noted however that, despite no differences being found in the whole population (beta diversity, difference in taxonomic abundance profiles from different samples), some significant modifications in the abundance of specific bacterial groups (alpha diversity) were detected. In fact, when analyzed by the data test ANCOM, specialized for microbiome, an increased abundance of *Allobaculum*, *Bifidobacterium* and *Lactobacillus* genus was detected, as well as a decreased abundance of *Odoribacter* and *Dehalobacterium* genus in LysM-GRK2$^{+/-}$ mice when compared with control littermates (Fig. S3a). On the other hand, when comparing 12 weeks of HFD vs 12 weeks of SD for each group, we found a similar decrease in alpha diversity in both genotypes, together with a significant increase in *Lactococcus* and decrease in *Prevotella* (Fig. S3b and c), suggesting that the identified changes reflect the influence of the HFD, and not so much of the genotype, on gut microbiota.

Since the HFD feeding induces a similar modulation of the microbiota in both LysM-GRK2$^{+/+}$ and LysM-GRK2$^{+/-}$ mice, we decided to analyze endotoxemia-induced changes in the glycemic response in LysM-GRK2$^{+/+}$ *vs* LysM-GRK2$^{+/-}$ mice. For this aim we injected mice with a low dose of bacterial endotoxin lipopolysaccharide (LPS, 1 mg/kg) and we found that the protection against glucose intolerance achieved by decreasing GRK2 levels in myeloid cells was maintained also in this acute pro-inflammatory model, at least at the level of LPS-induced hyperglycemia (Fig. S4), thus suggesting that the same degree of endotoxemia more severely impairs glucose metabolism in LysM-GRK2$^{+/+}$ than in LysM-GRK2$^{+/-}$ mice.

Altogether these results suggested that the observed differences in the inflammatory profile of tissues from HFD-fed control or LysM-GRK2$^{+/-}$ mice seem to depend on intrinsic properties of infiltrating macrophages with reduced levels of GRK2, which would respond in a different way

to pro-inflammatory stimuli, rather than to differences in microbiota.

Decreasing GRK2 levels in myeloid cells impairs pro-inflammatory responses in macrophages

In order to specifically study the inflammatory response of macrophages with decreased levels of GRK2, we used thioglycollate-elicited peritoneal macrophages (TEPMs) from LysM GRK2$^{+/+}$ and LysM GRK2$^{+/-}$ mice. In agreement with with previous results, LPS-induced enhancement of iNOS expression was lower in TEPMs from LysM GRK2$^{+/-}$ mice compared with GRK2$^{+/+}$ macrophages, as was also observed in TEPMs treated with the GRK2 inhibitor Cpd101 (Fig. 6a, b). This decreased expression of iNOS occurred in the absence of differences in LPS-induced COX2 expression, and was coincident with a decreased secretion of the main pro-inflammatory cytokines TNFα and IL-6, without differences in the secretion of the anti-inflammatory cytokine IL-10 (Fig. 6c). To explore whether this decreased proinflammatory response would have an impact in other cell types, we treated 3T3L1 adipocytes for 24 h with conditioned media (CM) from GRK2$^{+/+}$ or GRK2$^{+/-}$ macrophages stimulated or not with LPS, and evaluated their response to insulin by measuring the phosphorylation level of AKT. We found that insulin signaling was impaired in 3T3L1 adipocytes treated with the CM from LPS-stimulated GRK2$^{+/+}$ macrophages, whereas CM from LPS-stimulated GRK2$^{+/-}$ macrophages did not induce insulin resistance in these cells (Fig. 7a), what is in agreement with the decreased secretion of key pro-inflammatory cytokines by GRK2$^{+/-}$ macrophages upon LPS stimulation.

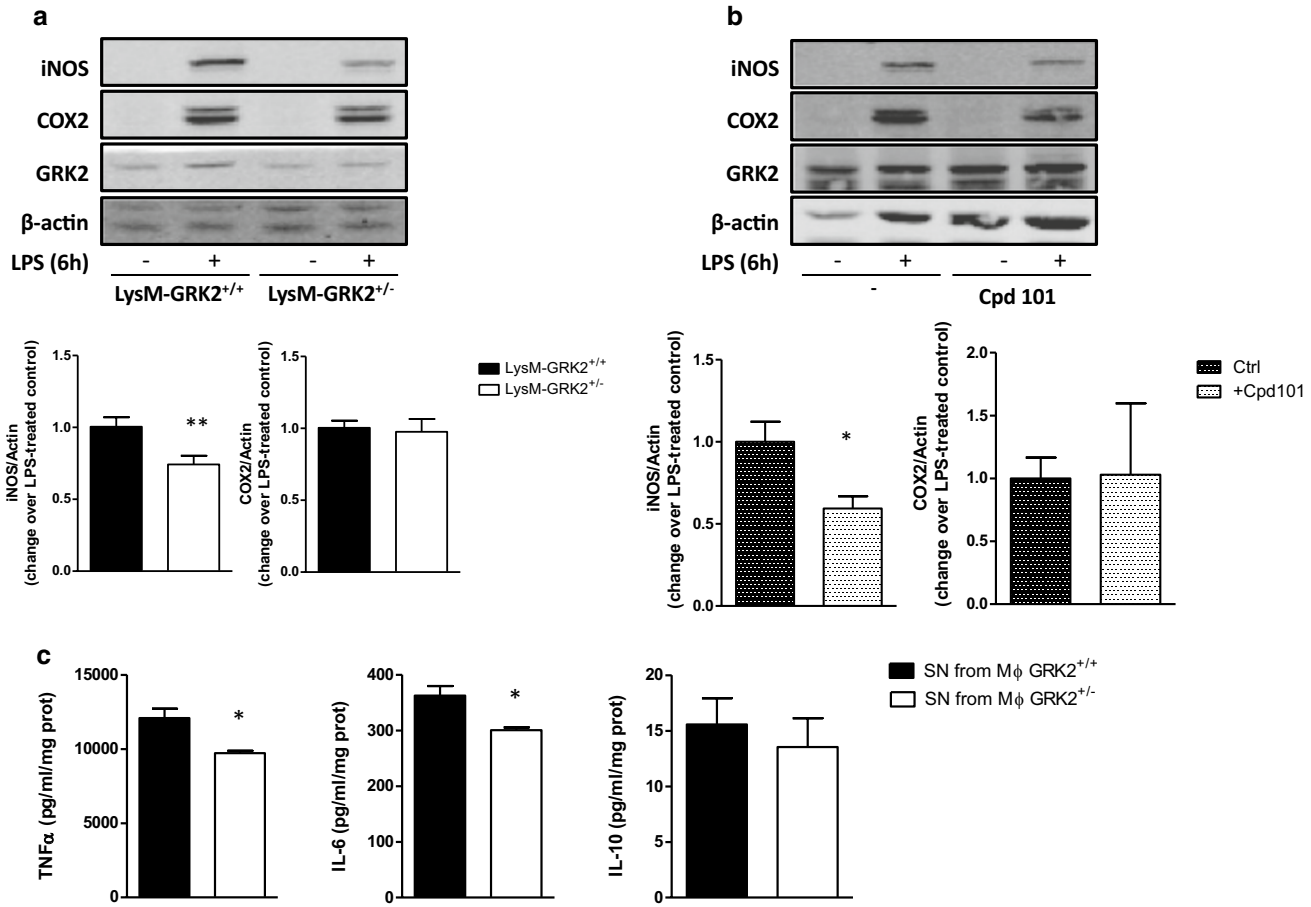

Fig. 6 Decreasing GRK2 levels diminishes pro-inflammatory activation of macrophages in vitro. **a** Thioglycollate-elicited peritoneal macrophages (TEPMs) isolated from either LysM-GRK2$^{+/+}$ or LysM-GRK2$^{+/-}$ mice were cultured for 2 days in RPMI supplemented with 10% FBS, serum-starved overnight and stimulated with 1 μg/ml LPS for 6 h. Lysates were analyzed by WB with the corresponding antibodies against iNOS (NOS-2), COX-2, GRK2 and β-actin. **b** WB results from TEPMs of control mice with the same treatment but in the absence or presence of the GRK2 inhibitor Cpd101 (30 μM). Lysates were analyzed by WB with the previously mentioned antibodies. Representative immunoblots of 3–6 independent experiments and densitometric analysis are shown. Results are expressed as fold change over LPS-stimulated control macrophages (control being GRK2$^{+/+}$ macrophages (**a**) or macrophages untreated with Cpd101 in (**b**). **c** Cytokines in the supernatants of GRK2$^{+/+}$ or GRK2$^{+/-}$ TEPMs were measured after 6 h of LPS (1 μg/ml) stimulation. Cytokine protein levels were normalized to the total amount of protein within each well (in mg), and results are means ± SEM of 4–6 experiments. Statistical significance was analyzed by unpaired two-tailed *t* test (*$p < 0.05$; **$p < 0.01$)

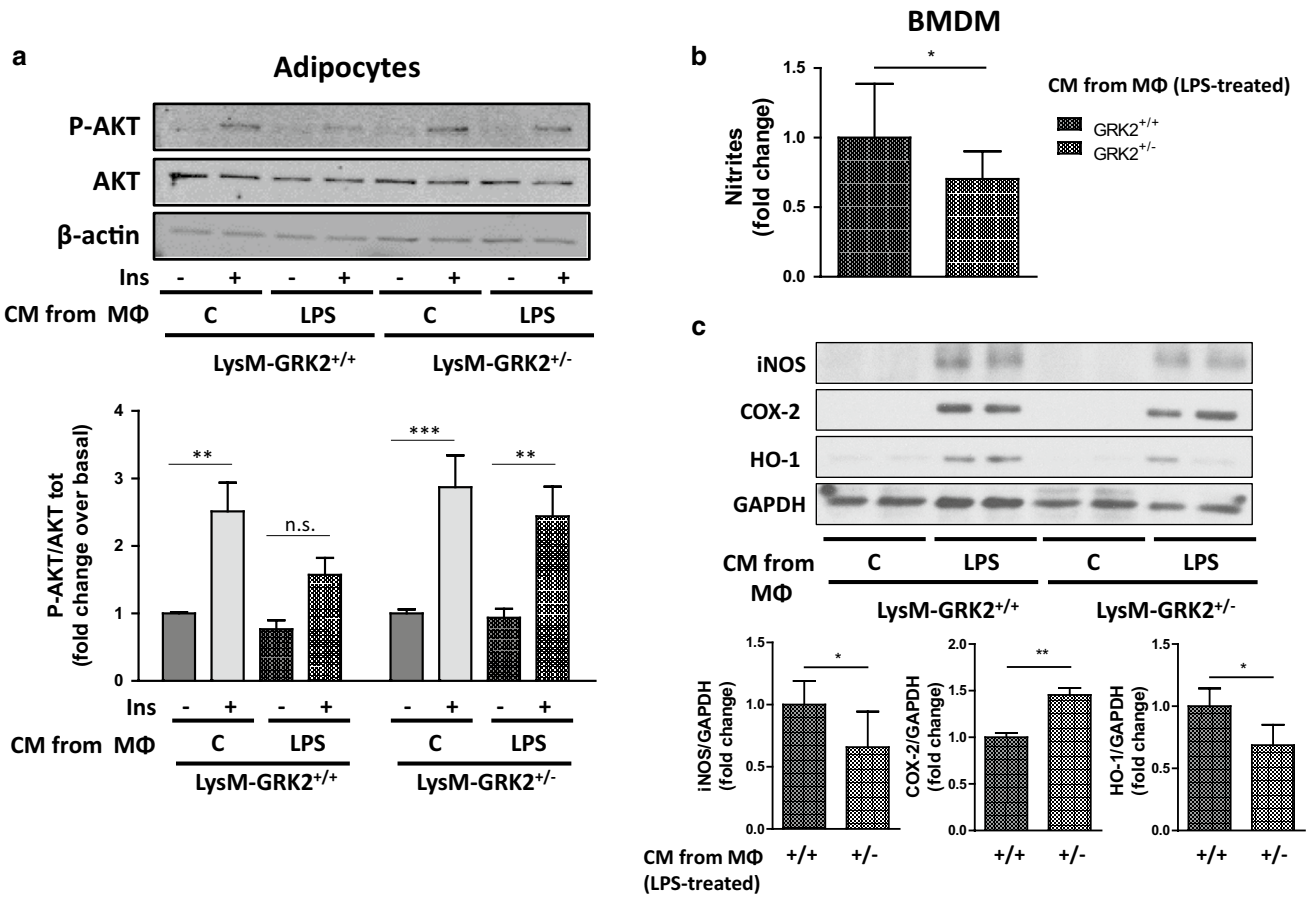

Fig. 7 Effect of the conditioned medium from thioglycollate-elicited peritoneal macrophages (TEPMs) isolated from either LysM-GRK2$^{+/+}$ or LysM-GRK2$^{+/-}$ mice on adipocytes and naïve bone-marrow-derived macrophages (BMDM). **a** 3T3L1 adipocytes were stimulated for 24 h with the conditioned medium (CM) obtained from TEPMs isolated from either LysM-GRK2$^{+/+}$ or LysM-GRK2$^{+/-}$ mice previously treated or not with 1 μg/ml LPS for 6 h. 24 h later, 3T3L1 adipocytes were stimulated with insulin (Ins,10 nM) for 10 min and cell lysates were subjected to WB using antibodies against total and phosphorylated AKT (Ser473) and β-actin. Representative immunoblots (upper panel) and densitometric analysis (lower panel) of three independent experiments are shown. Results are expressed as fold change over basal (3T3L1 cells stimulated with CM from TEPMs non-stimulated with LPS and in the absence of insulin). Statistical significance was analyzed by two-way ANOVA followed by Bonferroni *post-hoc* test (**$p<0.01$; ***$p<0.005$). **b** Relative nitrite levels produced by BMDM upon 24 h-stimulation with CM obtained from TEPMs isolated from either LysM-GRK2$^{+/+}$ or LysM-GRK2$^{+/-}$ mice previously treated with 1 μg/ml LPS for 6 h. Results are expressed as fold change of nitrite concentration in the supernatant of BMDM stimulated with the CM of LPS-treated GRK2$^{+/-}$ macrophages over control (supernatant of BMDM stimulated with the CM of LPS-treated GRK2$^{+/+}$ macrophages). **c** Representative immunoblots (upper panel) and densitometric analysis normalized to GAPDH levels (lower panel) of iNOS, COX-2, HO-1 and GAPDH from BMDM exposed for 24 h to CM from LysM-GRK2$^{+/+}$ or LysM-GRK2$^{+/-}$ TEPMs stimulated or not with 1 μg/ml LPS for 6 h.. Graphs represent fold change over control (supernatant of BMDM stimulated with the CM of LPS-treated GRK2$^{+/+}$ macrophages). Statistical significance was analyzed by unpaired two-tailed t test (*$p<0.05$; **$p<0.01$)

Naïve BMDM from WT mice were also stimulated for 24 h with the CM from control or LPS-treated GRK2$^{+/+}$ or GRK2$^{+/-}$ macrophages and nitrites accumulation in their culture medium was measured (Fig. 7b). Stimulation with CM from LPS-treated GRK2$^{+/-}$ macrophages induced NO synthesis by BMDM to a lesser extent than stimulation with CM from LPS-treated GRK2$^{+/+}$ macrophages. Accordingly, iNOS and HO-1 expression were enhanced in BMDM stimulated with the CM from LPS-treated GRK2$^{+/+}$ macrophages compared with BMDM stimulated with CM from LPS-treated GRK2$^{+/-}$ macrophages (Fig. 7c). Collectively, these data suggest that, when stimulated with LPS, the secretome of macrophages with decreased levels of GRK2 fails to induce the same degree of pathological responses in other cell types, such as insulin resistance in adipocytes or inflammation in naïve macrophages.

Discussion

In this study, we show that decreasing GRK2 levels specifically in cells from the myeloid lineage protects against the development of HFD-induced glycemic dysregulation.

Notably, LysM-GRK2$^{+/-}$ mice were protected against HFD-induced alterations including hyperglycemia and hyperinsulinemia, as well as from HFD-induced glucose intolerance, in the absence of statistically significant differences in body weight gain. Since this latter parameter strongly influences IR, models in which body weight is comparable between groups after the HFD might be considered advantageous to specifically investigate the contribution of inflammation to HFD-induced metabolic alterations without the confounding factor of differences in obesity.

Interestingly, the improved glucose metabolism in LysM-GRK2$^{+/-}$ mice was not associated with significant differences in systemic insulin sensitivity, but with an enhanced repression of hepatic gluconeogenesis (as reflected by the PTT), as well as with an enhanced adipose and hepatic insulin sensitivity and decreased adipocyte size and hepatic steatosis in the face of a HFD. Other works have shown an improvement of glucose tolerance in a context of decreased hepatic steatosis without differences in systemic IR [49, 50]. Our data support the hypothesis that systemic IR and obesity are not necessarily linked, similar to studies showing that obesity is not required for immune-mediated disruption in glucose tolerance [51] or those in which mice with increased or the same degree of obesity are protected from metabolic complications solely through an improved inflammatory profile in adipose tissue [18, 50]. Indeed, it has been demonstrated that inflammation is regulated in a different way in adipose tissue and in muscle [52], as is insulin sensitivity [53].

Accordingly, there are two main consequences of the HFD-feeding: IR, which might be more linked to a decreased response to insulin in the muscle (that would affect both groups of mice to the same extent), and a hampered hepatic control of glucose homeostasis, which seems to be more dependent on obesity-associated inflammation, which appears attenuated in LysM-GRK2$^{+/-}$ mice, along with an improved hepatic insulin response and decreased steatosis. In this regard, innate immunity is considered a major contributor to the pathophysiology of NAFLD, and there is strong evidence for the involvement of macrophages in the development of hepatic steatosis and inflammation [10]. Several studies suggest direct associations between adipose tissue and hepatic inflammation [54]. Specifically, pro-inflammatory macrophages within WAT have been suggested to fuel hepatic lipid accumulation (reviewed in [55]). Moreover a causal relationship has been established between macrophages within visceral WAT from obese animals and increased hepatic inflammation during liver steatosis conditions, since transplantation of donor visceral WAT from obese mice, and not from lean animals, is per se able to induce hepatic macrophage accumulation [56]. This fat-liver axis is considered to explain that, during obesity, the polarization of liver macrophages towards a pro-inflammatory phenotype is not the only important phenomenon for the development of NAFLD. Rather, WAT macrophages, especially those in the visceral compartment, may contribute to the development of hepatic IR and hepatosteatosis through their effects on chronic inflammation [10]. Indeed, the liver is the organ more exposed to cytokines released from visceral fat tissue, since these can be directly secreted into the portal vein of obese subjects to directly reach the liver [57]. The existence of this fat-liver crosstalk during obesity is also supported by data from several mouse models in which the disruption of inflammatory pathways specifically in adipocytes resulted in protection against diet-induced hepatic steatosis and IR [58, 59], while, in humans, recent studies have shown a relationship between IR in the adipose tissue and activation of hepatic macrophages in patients with NAFLD [60].

Interestingly, the visceral adipose tissue of LysM-GRK2$^{+/-}$ mice displays an enhanced insulin sensitivity, a decreased adipocyte size, increased expression of *Adiponectin* together with a decreased expression of *Leptin* and an attenuated inflammatory pattern compared to HFD-fed control littermates. Obesity-associated alterations in the aforementioned adipokines has been described to contribute importantly to the development of a dysfunctional adipose tissue as well as to directly impact on insulin sensitivity in the liver [61], and the adiponectin to leptin ratio has been suggested as a marker of adipose tissue dysfunction and IR (reviewed in [62]). Adiponectin has been reported to reduce inflammation, which may be associated with an amelioration of IR [63], and, specifically in the liver, it plays an important role in the inhibition of hepatic glucose production [64]. One of the characteristics of adipose tissue dysfunction is a proinflammatory macrophage polarization. In fact, adipose cell enlargement during obesity leads to an altered pattern of expression and secretion of adipokines, favoring a pro-inflammatory state with reduced levels of adiponectin and increased production of cytokines and chemokines, which impair insulin signaling [65, 66]. Importantly, we find that the visceral adipose tissue of HFD-fed LysM-GRK2$^{+/-}$ mice exhibits a decreased expression of key pro-inflammatory cytokines and an increased expression of adiponectin, suggestive of a less dysfunctional WAT in these animals. The expression of TNFα, one of the most important mediators of inflammation secreted by macrophages [61, 66] is decreased in adipose tissue from LysM-GRK2$^{+/-}$ mice, along with that of relevant markers of pro-inflammatory macrophages such as CCR2 and MCP-1 (CCL2). Accordingly, although we did not find significant differences in the total number of macrophages within adipose tissue, we noted a decreased presence of the pro-inflammatory M1 macrophages (F4/80^{+}CD11b^{+}CD11c^{+} cells). Thus, it is tempting to postulate that such decreased inflammatory pattern in WAT would relate to a decreased input of inflammatory cytokines to the

liver, in turn reducing activation of resident Kupffer cells and subsequent recruitment of macrophages to the liver in LysM-GRK2$^{+/-}$ mice, resulting in overall protection from IR and steatosis and preserved overall metabolic homeostasis.

In this regard, during a HFD, Kupffer cells are activated and initiate inflammation through the production of TNFα, IL-1β, IL-6 and chemoattractants, helping recruit neutrophils and circulating monocytes, which rapidly acquire a pro-inflammatory phenotype and further promote NAFLD progression [10]. Accordingly, the protection from hepatic steatosis that we find in LysM-GRK2$^{+/-}$ mice is accompanied by a decreased expression of pro-inflammatory cytokines as well as by a decreased presence of macrophages within the liver. These data suggest that decreasing GRK2 levels in myeloid cells can cause a decreased pro-inflammatory activation of Kupffer cells, a reduced recruitment and activation of circulating monocytes or both.

GRK2 has been shown to negatively regulate chemotactic responses through its canonical inhibitory role of chemokine GPCR signaling as occurs with classical chemokines as MIP-2 [28] or CCL2 [67]. This would speak against a reduced migratory capacity of macrophages as responsible for the decreased presence of macrophages in the liver of LysM-GRK2$^{+/-}$ mice. However, in certain contexts and cell types GRK2 may enhance cell motility, as in migration of T and B lymphocytes from blood into lymph nodes [68] or in epithelial cell migration [69]. In addition, given the important role for β-arrestin2-biased signaling in the regulation of CCR2 expression and recruitment of leukocytes to different tissues [70], a decrease in GRK2 levels may also impair GPCR phosphorylation and subsequent β-arrestin2 recruitment, leading to impaired cell migration. Therefore, the fact that decreased migration of macrophages inside the liver is taking place in our model cannot be completely ruled out.

Of note, our data show significant differences in macrophage number only in the liver, but not in WAT of LysM-GRK2$^{+/-}$ mice compared to control littermates. Thus, the decrease in macrophages within the liver could be more related to a decreased activation of resident Kupffer cells and the concomitant reduction in the recruitment of pro-inflammatory macrophages, rather than to an intrinsically decreased migratory capacity of macrophages with lower levels of GRK2. This notion is consistent with the trend to decreased levels of mRNA expression of MCP-1 (CCL2) and CCR2 in the liver of LysM-GRK2$^{+/-}$ mice. Interestingly, CCL2 mRNA expression has been described to be significantly upregulated in liver tissue from patients with NAFLD, and CCR2 antagonism reduces infiltration of CD11c^{+}F4/80^{+} cells into the liver in HFD-fed mice, accompanied by improvements in liver steatosis and glycemic control [71].

The observed differences in the inflammatory profile of LysM-GRK2$^{+/-}$ mice upon a HFD seem to arise from intrinsic properties of macrophages with reduced levels of GRK2. On the one hand, we did not find significant differences in the composition of gut microbiota between genotypes upon a HFD diet, suggesting that altered microbiota-derived LPS, a known driver for macrophage inflammation within WAT besides fatty acids, is not playing a major role. On the other hand, the reduced inflammatory status of LysM-GRK2$^{+/-}$ WAT was not accompanied by a decrease in macrophage abundance, consistent with the notion that decreasing GRK2 levels in myeloid cells per se impairs pro-inflammatory responses. The fact that the glycemic response to endotoxemia was differentially affected in LysM-GRK2$^{+/+}$ vs LysM-GRK2$^{+/-}$ mice also supports that the fact that the underlying cause of the differences observed in the inflammatory profile between genotypes should depend on intrinsic properties of macrophages with reduced levels of GRK2.

Consistent with this notion, the response to pro-inflammatory stimuli such as LPS is comparatively decreased in LysM-GRK2$^{+/-}$ macrophages both in terms of iNOS induction and cytokine production. Moreover, in BMDM, the decrease in NO production induced by the CM from LysM-GRK2$^{+/-}$ macrophages correlates with a decreased expression of HO-1, which has been reported to be induced via NO-induced nuclear translocation of Nrf2 in order to counteract iNOS expression and activity [72].

Interestingly, whereas decreased GRK2 dosage or catalytic inhibition attenuates LPS-induced iNOS expression, the concurrent up-modulation in COX-2 levels is not affected. LPS stimulates nuclear factor kB (NF-kB), an important transcription factor for both iNOS and COX-2 [73]. However, the regulation of the expression of these proteins in myeloid cell types in response to inflammatory stimuli is very complex and involves a variety of additional signaling networks, including MAPK cascades and STAT3 stimulation. Our results suggest that differential regulation mechanism of these proteins take place in macrophages with decreased levels of GRK2 upon LPS treatment that are yet to be elucidated.

Interestingly, despite being considered a pro-inflammatory enzyme, COX-2 also exerts biological activities that resolve inflammation [74, 75] by producing pro-resolving PGs such as PGD2, 15-deoxy-Δ12,14-PGJ2, and PGF2α [76]. Thus, it is tempting to speculate that downmodulation of GRK2 levels in macrophages, by decreasing iNOS while maintaining increased COX-2 levels, would favor an increased production of prostaglandins and pro-resolving derivatives. One of those, 15d-PGJ$_2$ has been reported to downmodulate the inflammatory response [77] and shows an inhibitory effect that is preferential over iNOS compared with COX-2 expression in LPS-activated macrophages [78]. 15d-PGJ$_2$ has also been described to reduce pro-inflammatory cytokine expression [79]. GRK2 down-modulation may also foster the response to PGE2, which also has anti-inflammatory effects [80] mainly mediated by the EP4 receptor,

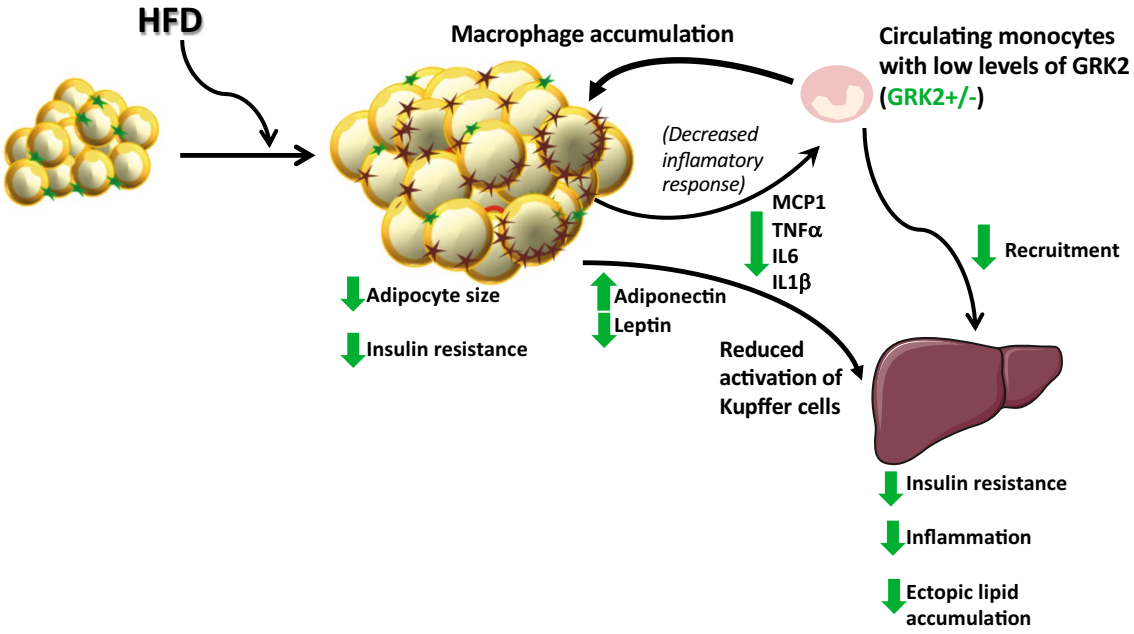

Fig. 8 Effect of lowering GRK2 levels in myeloid cells in the modulation of the adipose-liver crosstalk. In obesity, chemokines stimulate the infiltration of macrophages into the WAT promoting a pro-inflammatory phenotype in adipose tissue macrophages, which contribute to the development of a persistent, low-grade inflammation. Pro-inflammatory mediators in WAT induce IR and further enhance monocyte recruitment, perpetuating a self-fed cycle of inflammation and altering adipokine expression pattern. The dysfunctional WAT and its infiltrating pro-inflammatory macrophages fuel hepatic IR, lipid accumulation and the activation of Kupffer cells within the liver. Decreased levels of GRK2 in myeloid cells reduce the pro-inflammatory response of macrophages in the face of a HFD, fostering a less inflamed adipose tissue, a preserved adipokine secretion pattern, and a decreased expression of inflammatory cytokines. This reduces activation of Kupffer cells and subsequent recruitment of macrophages in the liver, protects from IR and steatosis and preserves overall metabolic homeostasis. Arrows represent the effect of lowering GRK2 on the different processes. Stars represent M2 (green) or M1 (brown) macrophages

which is desensitized by GRK2 [81]. Reduced GRK2 dosage may also favor in vivo the action of endogenous catecholamines acting through β-adrenergic receptors in macrophages that are able to counteract LPS-induced inflammation and M1 polarization [82–84]. Thus, either an increased production of pro-resolving prostaglandin derivatives or an increased response to anti-inflammatory PGE2 or catecholamines may contribute to the reduced pro-inflammatory capacity of macrophages with reduced levels of GRK2.

GRK2 is highly expressed in different cell types of the immune system, and its levels and activity are differentially altered in a number of inflammatory pathologies [31], what suggests that GRK2 is an important regulator of cell responses during inflammation. However, the role of GRK2 specifically in macrophages is controversial, with reports describing opposing LPS-driven outcomes in macrophages with altered levels/activity of GRK2 [85–87]. This apparent discrepancy can be explained by differences in the precise degree of GRK2 inhibition or silencing, the experimental model utilized (model cell lines or macrophages isolated from the peritoneal cavity by different procedures), or the dose and duration of LPS stimulation. Adding additional complexity, GRK2 can modulate a variety of pathways related to inflammation so the impact of its downmodulation might be differentially integrated in distinct contexts. Specifically in myeloid cells, decreased GRK2 has been reported to enhance stimulation of p38 MAPK [86, 87] or to enhance ERK1/2 signaling [85]) to foster inflammation. In other reports in line with our data, GRK2 knockdown in macrophages inhibits TNFα-induced NFκB-dependent gene transcription in macrophages, thus blocking expression of inflammatory genes [88], and the ablation/inhibition of GRK2 prevented ROS generation and iNOS induction in LPS-stimulated microglial cells by modulating STAT3 phosphorylation and IRF1 activity [89, 90]. In our experimental contexts, the anti-inflammatory mechanisms triggered by reduced GRK2 expression appear to predominate, helping to maintain inflammation at bay in HFD-related pathologies.

In sum, our data uncover that partially decreasing GRK2 levels in myeloid cells, by modulating macrophage pro-inflammatory ability, has an impact on inter-organ crosstalk particularly between WAT and the liver that is able to prevent obesity-related NAFLD and hepatic IR and to improve systemic glucose homeostasis (see Fig. 8). Our data also reinforce the key role of the innate immune system and its

modulation by GRK2 in metabolic homeostasis and tissue coordination in obesity-related pathological contexts.

Acknowledgements We acknowledge support by Ministerio de Economía y Competitividad (MINECO/FEDER), Spain (grant SAF2017-84125-R to FM and CM and SAF2017-82436R to LB); CIBER de Enfermedades Cardiovasculares (CIBERCV). Instituto de Salud Carlos III, Spain (grant CB16/11/00278 to F.M., CB16/11/00222 to L.B., and, PI15/01114 to Francisco Tinaones (Universidad De Málaga, Spain), co-funded with European FEDER contribution); European Foundation for the Study of Diabetes (EFSD) Novo Nordisk Partnership for Diabetes Research in Europe Grant (to F.M.); and Programa de Actividades en Biomedicina de la Comunidad de Madrid-B2017/BMD-3671-INFLAMUNE to FM and MF.. I.M.-I. was supported by the "MS type I" program (CP16/00163). The authors thank the Metagenomic Platform of the Centro de Investigación Biomédica en Red de Fisiopatología de la Obesidad y la Nutrición, CIBERobn, Instituto de Salud Carlos III (ISCIII), Spain. We appreciate the help of the CBMSO Facilities, in particular Flow Cytometry, Genomics and Animal Care. We acknowledge Paula Ramos for technical support. We also acknowledge the institutional support to the CBMSO from Fundación Ramón Areces.

References

1. Younossi Z, Tacke F, Arrese M, Sharma BC, Mostafa I, Bugianesi E, Wong VW, Yilmaz Y, George J, Fan J, Vos MB (2018) Global perspectives on non-alcoholic fatty liver disease and non-alcoholic steatohepatitis. Hepatology. https://doi.org/10.1002/hep.30251
2. Rosen ED, Spiegelman BM (2014) What we talk about when we talk about fat. Cell 156(1–2):20–44. https://doi.org/10.1016/j.cell.2013.12.012
3. Donath MY, Shoelson SE (2011) Type 2 diabetes as an inflammatory disease. Nat Rev Immunol 11(2):98–107. https://doi.org/10.1038/nri2925
4. Lumeng CN, Bodzin JL, Saltiel AR (2007) Obesity induces a phenotypic switch in adipose tissue macrophage polarization. J Clin Investig 117(1):175–184. https://doi.org/10.1172/JCI29881
5. Lumeng CN, DelProposto JB, Westcott DJ, Saltiel AR (2008) Phenotypic switching of adipose tissue macrophages with obesity is generated by spatiotemporal differences in macrophage subtypes. Diabetes 57(12):3239–3246. https://doi.org/10.2337/db08-0872
6. Olefsky JM, Glass CK (2010) Macrophages, inflammation, and insulin resistance. Annu Rev Physiol 72:219–246. https://doi.org/10.1146/annurev-physiol-021909-135846
7. Odegaard JI, Chawla A (2008) Mechanisms of macrophage activation in obesity-induced insulin resistance. Nat Clin Pract Endocrinol Metab 4(11):619–626. https://doi.org/10.1038/ncpendmet0976
8. Cusi K (2012) Role of obesity and lipotoxicity in the development of nonalcoholic steatohepatitis: pathophysiology and clinical implications. Gastroenterology 142(4):711–725. https://doi.org/10.1053/j.gastro.2012.02.003
9. van der Poorten D, Milner KL, Hui J, Hodge A, Trenell MI, Kench JG, London R, Peduto T, Chisholm DJ, George J (2008) Visceral fat: a key mediator of steatohepatitis in metabolic liver disease. Hepatology 48(2):449–457. https://doi.org/10.1002/hep.22350
10. Kazankov K, Jorgensen SMD, Thomsen KL, Moller HJ, Vilstrup H, George J, Schuppan D, Gronbaek H (2019) The role of macrophages in nonalcoholic fatty liver disease and nonalcoholic steatohepatitis. Nat Rev Gastroenterol Hepatol 16(3):145–159. https://doi.org/10.1038/s41575-018-0082-x
11. Gregor MF, Hotamisligil GS (2011) Inflammatory mechanisms in obesity. Annu Rev Immunol 29:415–445. https://doi.org/10.1146/annurev-immunol-031210-101322
12. Ouchi N, Parker JL, Lugus JJ, Walsh K (2011) Adipokines in inflammation and metabolic disease. Nat Rev Immunol 11(2):85–97. https://doi.org/10.1038/nri2921
13. Weisberg SP, McCann D, Desai M, Rosenbaum M, Leibel RL, Ferrante AW Jr (2003) Obesity is associated with macrophage accumulation in adipose tissue. J Clin Investig 112(12):1796–1808. https://doi.org/10.1172/JCI19246
14. Cani PD, Everard A, Duparc T (2013) Gut microbiota, enteroendocrine functions and metabolism. Curr Opin Pharmacol 13(6):935–940. https://doi.org/10.1016/j.coph.2013.09.008
15. Shen J, Obin MS, Zhao L (2013) The gut microbiota, obesity and insulin resistance. Mol Aspects Med 34(1):39–58. https://doi.org/10.1016/j.mam.2012.11.001
16. Musso G, Gambino R, Cassader M (2011) Interactions between gut microbiota and host metabolism predisposing to obesity and diabetes. Annu Rev Med 62:361–380. https://doi.org/10.1146/annurev-med-012510-175505
17. Cani PD, Amar J, Iglesias MA, Poggi M, Knauf C, Bastelica D, Neyrinck AM, Fava F, Tuohy KM, Chabo C, Waget A, Delmee E, Cousin B, Sulpice T, Chamontin B, Ferrieres J, Tanti JF, Gibson GR, Casteilla L, Delzenne NM, Alessi MC, Burcelin R (2007) Metabolic endotoxemia initiates obesity and insulin resistance. Diabetes 56(7):1761–1772. https://doi.org/10.2337/db06-1491
18. Shi H, Kokoeva MV, Inouye K, Tzameli I, Yin H, Flier JS (2006) TLR4 links innate immunity and fatty acid-induced insulin resistance. J Clin Investig 116(11):3015–3025. https://doi.org/10.1172/JCI28898
19. Nguyen MT, Favelyukis S, Nguyen AK, Reichart D, Scott PA, Jenn A, Liu-Bryan R, Glass CK, Neels JG, Olefsky JM (2007) A subpopulation of macrophages infiltrates hypertrophic adipose tissue and is activated by free fatty acids via Toll-like receptors 2 and 4 and JNK-dependent pathways. J Biolog Chem 282(48):35279–35292. https://doi.org/10.1074/jbc.M706762200
20. Biswas SK, Mantovani A (2012) Orchestration of metabolism by macrophages. Cell Metab 15(4):432–437. https://doi.org/10.1016/j.cmet.2011.11.013
21. Ribas C, Penela P, Murga C, Salcedo A, Garcia-Hoz C, Jurado-Pueyo M, Aymerich I, Mayor F Jr (2007) The G protein-coupled receptor kinase (GRK) interactome: role of GRKs in GPCR regulation and signaling. Biochem Biophys Acta 1768(4):913–922. https://doi.org/10.1016/j.bbamem.2006.09.019
22. Hullmann J, Traynham CJ, Coleman RC, Koch WJ (2016) The expanding GRK interactome: Implications in cardiovascular disease and potential for therapeutic development. Pharmacol Res 110:52–64. https://doi.org/10.1016/j.phrs.2016.05.008
23. Penela P, Lafarga V, Tapia O, Rivas V, Nogues L, Lucas E, Vila-Bedmar R, Murga C, Mayor F Jr (2012) Roles of GRK2 in cell signaling beyond GPCR desensitization GRK2HDAC6 interaction modulates cell spreading and motility. Sci Signal 5(224):9–10. https://doi.org/10.1126/scisignal.2003098
24. Penela P, Murga C, Ribas C, Lafarga V, Mayor F Jr (2010) The complex G protein-coupled receptor kinase 2 (GRK2) interactome unveils new physiopathological targets. Br J Pharmacol 160(4):821–832. https://doi.org/10.1111/j.1476-5381.2010.00727.x
25. Anis Y, Leshem O, Reuveni H, Wexler I, Ben Sasson R, Yahalom B, Laster M, Raz I, Ben Sasson S, Shafrir E, Ziv E (2004) Antidiabetic effect of novel modulating peptides of G-protein-coupled kinase in experimental models of diabetes. Diabetologia 47(7):1232–1244. https://doi.org/10.1007/s00125-004-1444-1

26. Mayor F Jr, Lucas E, Jurado-Pueyo M, Garcia-Guerra L, Nieto-Vazquez I, Vila-Bedmar R, Fernandez-Veledo S, Murga C (2011) G Protein-coupled receptor kinase 2 (GRK2): a novel modulator of insulin resistance. Arch Physiol Biochem 117(3):125–130. https://doi.org/10.3109/13813455.2011.584693
27. Ciccarelli M, Cipolletta E, Iaccarino G (2012) GRK2 at the control shaft of cellular metabolism. Curr Pharm Des 18(2):121–127
28. Fan J, Malik AB (2003) Toll-like receptor-4 (TLR4) signaling augments chemokine-induced neutrophil migration by modulating cell surface expression of chemokine receptors. Nat Med 9(3):315–321. https://doi.org/10.1038/nm832
29. Loniewski K, Shi Y, Pestka J, Parameswaran N (2008) Toll-like receptors differentially regulate GPCR kinases and arrestins in primary macrophages. Mol Immunol 45(8):2312–2322. https://doi.org/10.1016/j.molimm.2007.11.012
30. Lombardi MS, Kavelaars A, Penela P, Scholtens EJ, Roccio M, Schmidt RE, Schedlowski M, Mayor F Jr, Heijnen CJ (2002) Oxidative stress decreases G protein-coupled receptor kinase 2 in lymphocytes via a calpain-dependent mechanism. Mol Pharmacol 62(2):379–388
31. Vroon A, Heijnen CJ, Kavelaars A (2006) GRKs and arrestins: regulators of migration and inflammation. J Leukoc Biol 80(6):1214–1221. https://doi.org/10.1189/jlb.0606373
32. Clausen BE, Burkhardt C, Reith W, Renkawitz R, Forster I (1999) Conditional gene targeting in macrophages and granulocytes using LysMcre mice. Transgen Res 8(4):265–277
33. Willemen HL, Eijkelkamp N, Wang H, Dantzer R, Dorn GW 2nd, Kelley KW, Heijnen CJ, Kavelaars A (2010) Microglial/macrophage GRK2 determines duration of peripheral IL-1beta-induced hyperalgesia: contribution of spinal cord CX3CR1, p38 and IL-1 signaling. Pain 150(3):550–560. https://doi.org/10.1016/j.pain.2010.06.015
34. Rivas V, Carmona R, Munoz-Chapuli R, Mendiola M, Nogues L, Reglero C, Miguel-Martin M, Garcia-Escudero R, Dorn GW 2nd, Hardisson D, Mayor F Jr, Penela P (2013) Developmental and tumoral vascularization is regulated by G protein-coupled receptor kinase 2. J Clin Investig 123(11):4714–4730. https://doi.org/10.1172/JCI67333
35. Vila-Bedmar R, Cruces-Sande M, Lucas E, Willemen HL, Heijnen CJ, Kavelaars A, Mayor F, Murga C (2015) Reversal of diet-induced obesity and insulin resistance by inducible genetic ablation of GRK2. Science Signal 8(386):9–10. https://doi.org/10.1126/scisignal.aaa4374
36. Cruces-Sande M, Vila-Bedmar R, Arcones AC, Gonzalez-Rodriguez A, Rada P, Gutierrez-de-Juan V, Vargas-Castrillon J, Iruzubieta P, Sanchez-Gonzalez C, Formentini L, Crespo J, Garcia-Monzon C, Martinez-Chantar ML, Valverde AM, Mayor F Jr (1864) Murga C (2018) Involvement of G protein-coupled receptor kinase 2 (GRK2) in the development of non-alcoholic steatosis and steatohepatitis in mice and humans. Biochim Biophys Acta Mol Basis Dis 12:3655–3667. https://doi.org/10.1016/j.bbadis.2018.09.027
37. Callahan BJ, McMurdie PJ, Rosen MJ, Han AW, Johnson AJA, Holmes SP (2016) DADA2: high resolution sample inference from Illumina amplicon data. Nat Methods 13(7):581–583. https://doi.org/10.1038/nmeth.3869
38. Bolyen ERJ, Dillon MR, Bokulich NA, Abnet C, Al-Ghalith GA, Alexander H, Alm EJ, Arumugam M, Asnicar F, Bai Y, Bisanz JE, Bittinger K, Brejnrod A, Brislawn CJ, Brown CT, Callahan BJ, Caraballo-Rodríguez AM, Chase J, Cope E, Da Silva R, Dorrestein PC, Douglas GM, Durall DM, Duvallet C, Edwardson CF, Ernst M, Estaki M, Fouquier J, Gauglitz JM, Gibson DL, Gonzalez A, Gorlick K, Guo J, Hillmann B, Holmes S, Holste H, Huttenhower C, Huttley G, Janssen S, Jarmusch AK, Jiang L, Kaehler B, Kang KB, Keefe CR, Keim P, Kelley ST, Knights D, Koester I, Kosciolek T, Kreps J, Langille MG, Lee J, Ley R, Liu Y, Loftfield E, Lozupone C, Maher M, Marotz C, Martin BD, McDonald D, McIver LJ, Melnik AV, Metcalf JL, Morgan SC, Morton J, Naimey AT, Navas-Molina JA, Nothias LF, Orchanian SB, Pearson T, Peoples SL, Petras D, Preuss ML, Pruesse E, Rasmussen LB, Rivers A, Robeson MS II, Rosenthal P, Segata N, Shaffer M, Shiffer A, Sinha R, Song SJ, Spear JR, Swafford AD, Thompson LR, Torres PJ, Trinh P, Tripathi A, Turnbaugh PJ, Ul-Hasan S, van der Hooft JJ, Vargas F, Vázquez-Baeza Y, Vogtmann E, von Hippel M, Walters W, Wan Y, Wang M, Warren J, Weber KC, Williamson CH, Willis AD, Xu ZZ, Zaneveld JR, Zhang Y, Zhu Q, Knight R, Caporaso JG (2018) QIIME 2: Reproducible, interactive, scalable, and extensible microbiome data science. PeerJ Prepr 6:27292–27295. https://doi.org/10.7287/peerj.preprints.27295v2
39. Rognes T, Flouri T, Nichols B, Quince C, Mahé F (2016) VSEARCH: a versatile open source tool for metagenomics. PeerJ 4:e2584. https://doi.org/10.7717/peerj.2584
40. Mandal S, Van Treuren W, White RA, Eggesbø M, Knight R, Peddada SD (2015) Analysis of composition of microbiomes: a novel method for studying microbial composition. Microb Ecol Health Dis 26(1):27663. https://doi.org/10.3402/mehd.v26.27663
41. Maganto-Garcia E, Punzon C, Terhorst C, Fresno M (2008) Rab5 activation by Toll-like receptor 2 is required for *Trypanosoma cruzi* internalization and replication in macrophages. Traffic 9(8):1299–1315. https://doi.org/10.1111/j.1600-0854.2008.00760.x
42. Vila-Bedmar R, Garcia-Guerra L, Nieto-Vazquez I, Mayor F Jr, Lorenzo M, Murga C, Fernandez-Veledo S (2012) GRK2 contribution to the regulation of energy expenditure and brown fat function. FASEB J 26(8):3503–3514. https://doi.org/10.1096/fj.11-202267
43. Vila-Bedmar R, Lorenzo M, Fernandez-Veledo S (2010) Adenosine 5'-monophosphate-activated protein kinase-mammalian target of rapamycin cross talk regulates brown adipocyte differentiation. Endocrinology 151(3):980–992. https://doi.org/10.1210/en.2009-0810
44. Hatting M, Tavares CDJ, Sharabi K, Rines AK, Puigserver P (2018) Insulin regulation of gluconeogenesis. Ann N Y Acad Sci 1411(1):21–35. https://doi.org/10.1111/nyas.13435
45. Cai D, Yuan M, Frantz DF, Melendez PA, Hansen L, Lee J, Shoelson SE (2005) Local and systemic insulin resistance resulting from hepatic activation of IKK-beta and NF-kappaB. Nat Med 11(2):183–190. https://doi.org/10.1038/nm1166
46. Wan X, Xu C, Yu C, Li Y (2016) Role of NLRP3 Inflammasome in the Progression of NAFLD to NASH. Can J Gastroenterol Hepatol 2016:6489012. https://doi.org/10.1155/2016/6489012
47. Hersoug LG, Moller P, Loft S (2016) Gut microbiota-derived lipopolysaccharide uptake and trafficking to adipose tissue: implications for inflammation and obesity. Obesity Rev 17(4):297–312. https://doi.org/10.1111/obr.12370
48. Ley RE, Backhed F, Turnbaugh P, Lozupone CA, Knight RD, Gordon JI (2005) Obesity alters gut microbial ecology. Proc Natl Acad Sci USA 102(31):11070–11075. https://doi.org/10.1073/pnas.0504978102
49. Moran-Salvador E, Lopez-Parra M, Garcia-Alonso V, Titos E, Martinez-Clemente M, Gonzalez-Periz A, Lopez-Vicario C, Barak Y, Arroyo V, Claria J (2011) Role for PPARgamma in obesity-induced hepatic steatosis as determined by hepatocyte- and macrophage-specific conditional knockouts. FASEB J 25(8):2538–2550. https://doi.org/10.1096/fj.10-173716
50. Poggi M, Bastelica D, Gual P, Iglesias MA, Gremeaux T, Knauf C, Peiretti F, Verdier M, Juhan-Vague I, Tanti JF, Burcelin R, Alessi MC (2007) C3H/HeJ mice carrying a toll-like receptor 4 mutation are protected against the development of insulin resistance in white adipose tissue in response to a high-fat diet. Diabetologia 50(6):1267–1276. https://doi.org/10.1007/s00125-007-0654-8

51. Bronsart LL, Contag CH (2016) A role of the adaptive immune system in glucose homeostasis. BMJ Open Diabetes Res Care 4(1):e000136. https://doi.org/10.1136/bmjdrc-2015-000136
52. Bruun JM, Helge JW, Richelsen B, Stallknecht B (2006) Diet and exercise reduce low-grade inflammation and macrophage infiltration in adipose tissue but not in skeletal muscle in severely obese subjects. Am J Physiol Endocrinol Metab 290(5):E961–967. https://doi.org/10.1152/ajpendo.00506.2005
53. Norris AW, Chen L, Fisher SJ, Szanto I, Ristow M, Jozsi AC, Hirshman MF, Rosen ED, Goodyear LJ, Gonzalez FJ, Spiegelman BM, Kahn CR (2003) Muscle-specific PPARgamma-deficient mice develop increased adiposity and insulin resistance but respond to thiazolidinediones. J Clin Investig 112(4):608–618. https://doi.org/10.1172/JCI17305
54. Stanton MC, Chen SC, Jackson JV, Rojas-Triana A, Kinsley D, Cui L, Fine JS, Greenfeder S, Bober LA, Jenh CH (2011) Inflammatory Signals shift from adipose to liver during high fat feeding and influence the development of steatohepatitis in mice. J Inflamm (Lond) 8:8. https://doi.org/10.1186/1476-9255-8-8
55. Lefere S, Tacke F (2019) Macrophages in obesity and non-alcoholic fatty liver disease: crosstalk with metabolism. JHEP Rep 1(1):30–43. https://doi.org/10.1016/j.jhepr.2019.02.004
56. Bijnen M, Josefs T, Cuijpers I, Maalsen CJ, van de Gaar J, Vroomen M, Wijnands E, Rensen SS, Greve JWM, Hofker MH, Biessen EAL, Stehouwer CDA, Schalkwijk CG, Wouters K (2018) Adipose tissue macrophages induce hepatic neutrophil recruitment and macrophage accumulation in mice. Gut 67(7):1317–1327. https://doi.org/10.1136/gutjnl-2016-313654
57. Rytka JM, Wueest S, Schoenle EJ, Konrad D (2011) The portal theory supported by venous drainage-selective fat transplantation. Diabetes 60(1):56–63. https://doi.org/10.2337/db10-0697
58. Sabio G, Das M, Mora A, Zhang Z, Jun JY, Ko HJ, Barrett T, Kim JK, Davis RJ (2008) A stress signaling pathway in adipose tissue regulates hepatic insulin resistance. Science 322(5907):1539–1543. https://doi.org/10.1126/science.1160794
59. Wueest S, Rapold RA, Schumann DM, Rytka JM, Schildknecht A, Nov O, Chervonsky AV, Rudich A, Schoenle EJ, Donath MY, Konrad D (2010) Deletion of Fas in adipocytes relieves adipose tissue inflammation and hepatic manifestations of obesity in mice. J Clin Investig 120(1):191–202. https://doi.org/10.1172/JCI38388
60. Rosso C, Kazankov K, Younes R, Esmaili S, Marietti M, Sacco M, Carli F, Gaggini M, Salomone F, Moller HJ, Abate ML, Vilstrup H, Gastaldelli A, George J, Gronbaek H, Bugianesi E (2019) Crosstalk between adipose tissue insulin resistance and liver macrophages in non-alcoholic fatty liver disease. J Hepatol 71(5):1012–1021. https://doi.org/10.1016/j.jhep.2019.06.031
61. Andersson CX, Gustafson B, Hammarstedt A, Hedjazifar S, Smith U (2008) Inflamed adipose tissue, insulin resistance and vascular injury. Diabetes Metab Res Rev 24(8):595–603. https://doi.org/10.1002/dmrr.889
62. Fruhbeck G, Catalan V, Rodriguez A, Gomez-Ambrosi J (2018) Adiponectin-leptin ratio: a promising index to estimate adipose tissue dysfunction. Relation with obesity-associated cardiometabolic risk. Adipocyte 7(1):57–62. https://doi.org/10.1080/21623945.2017.1402151
63. Kadowaki T, Yamauchi T, Kubota N, Hara K, Ueki K, Tobe K (2006) Adiponectin and adiponectin receptors in insulin resistance, diabetes, and the metabolic syndrome. J Clin Investig 116(7):1784–1792. https://doi.org/10.1172/JCI29126
64. Combs TP, Marliss EB (2014) Adiponectin signaling in the liver. Rev Endocr Metab Disord 15(2):137–147. https://doi.org/10.1007/s11154-013-9280-6
65. Gustafson B, Hammarstedt A, Andersson CX, Smith U (2007) Inflamed adipose tissue: a culprit underlying the metabolic syndrome and atherosclerosis. Arterioscler Thromb Vasc Biol 27(11):2276–2283. https://doi.org/10.1161/ATVBAHA.107.147835
66. Gustafson B (2010) Adipose tissue, inflammation and atherosclerosis. J Atheroscler Thromb 17(4):332–341
67. Liu Z, Jiang Y, Li Y, Wang J, Fan L, Scott MJ, Xiao G, Li S, Billiar TR, Wilson MA, Fan J (2013) TLR4 Signaling augments monocyte chemotaxis by regulating G protein-coupled receptor kinase 2 translocation. J Immunol 191(2):857–864. https://doi.org/10.4049/jimmunol.1300790
68. Arnon TI, Xu Y, Lo C, Pham T, An J, Coughlin S, Dorn GW, Cyster JG (2011) GRK2-dependent S1PR1 desensitization is required for lymphocytes to overcome their attraction to blood. Science 333(6051):1898–1903. https://doi.org/10.1126/science.1208248
69. Penela P, Ribas C, Aymerich I, Eijkelkamp N, Barreiro O, Heijnen CJ, Kavelaars A, Sanchez-Madrid F, Mayor F Jr (2008) G protein-coupled receptor kinase 2 positively regulates epithelial cell migration. EMBO J 27(8):1206–1218. https://doi.org/10.1038/emboj.2008.55
70. Grisanti LA, Traynham CJ, Repas AA, Gao E, Koch WJ, Tilley DG (2016) beta2-Adrenergic receptor-dependent chemokine receptor 2 expression regulates leukocyte recruitment to the heart following acute injury. Proc Natl Acad Sci USA 113(52):15126–15131. https://doi.org/10.1073/pnas.1611023114
71. Parker R, Weston CJ, Miao Z, Corbett C, Armstrong MJ, Ertl L, Ebsworth K, Walters MJ, Baumart T, Newland D, McMahon J, Zhang P, Singh R, Campbell J, Newsome PN, Charo I, Schall TJ, Adams DH (2018) CC chemokine receptor 2 promotes recruitment of myeloid cells associated with insulin resistance in nonalcoholic fatty liver disease. Am J Physiol Gastrointest Liver Physiol 314(4):G483–G493. https://doi.org/10.1152/ajpgi.00213.2017
72. Ashino T, Yamanaka R, Yamamoto M, Shimokawa H, Sekikawa K, Iwakura Y, Shioda S, Numazawa S, Yoshida T (2008) Negative feedback regulation of lipopolysaccharide-induced inducible nitric oxide synthase gene expression by heme oxygenase-1 induction in macrophages. Mol Immunol 45(7):2106–2115. https://doi.org/10.1016/j.molimm.2007.10.011
73. Tak PP, Firestein GS (2001) NF-kappaB: a key role in inflammatory diseases. J Clin Investig 107(1):7–11. https://doi.org/10.1172/JCI11830
74. Rajakariar R, Yaqoob MM, Gilroy DW (2006) COX-2 in inflammation and resolution. Mol Interv 6(4):199–207. https://doi.org/10.1124/mi.6.4.6
75. Gilroy DW, Colville-Nash PR, Willis D, Chivers J, Paul-Clark MJ, Willoughby DA (1999) Inducible cyclooxygenase may have anti-inflammatory properties. Nat Med 5(6):698–701. https://doi.org/10.1038/9550
76. Gao Y, Zhang H, Luo L, Lin J, Li D, Zheng S, Huang H, Yan S, Yang J, Hao Y, Li H, Gao Smith F, Jin S (2017) Resolvin D1 Improves the Resolution of Inflammation via Activating NF-kappaB p50/p50-Mediated Cyclooxygenase-2 Expression in Acute Respiratory Distress Syndrome. J Immunol. https://doi.org/10.4049/jimmunol.1700315
77. Scher JU, Pillinger MH (2005) 15d-PGJ2: the anti-inflammatory prostaglandin? Clin Immunol 114(2):100–109. https://doi.org/10.1016/j.clim.2004.09.008
78. Tsoyi K, Ha YM, Kim YM, Lee YS, Kim HJ, Kim HJ, Seo HG, Lee JH, Chang KC (2009) Activation of PPAR-gamma by carbon monoxide from CORM-2 leads to the inhibition of iNOS but not COX-2 expression in LPS-stimulated macrophages. Inflammation 32(6):364–371. https://doi.org/10.1007/s10753-009-9144-0
79. Han Z, Zhu T, Liu X, Li C, Yue S, Liu X, Yang L, Yang L, Li L (2012) 15-deoxy-Delta 12,14 -prostaglandin J2 reduces recruitment of bone marrow-derived monocyte/macrophages in chronic

liver injury in mice. Hepatology 56(1):350–360. https://doi.org/10.1002/hep.25672
80. Takayama K, Garcia-Cardena G, Sukhova GK, Comander J, Gimbrone MA Jr, Libby P (2002) Prostaglandin E2 suppresses chemokine production in human macrophages through the EP4 receptor. J Biolog Chem 277(46):44147–44154. https://doi.org/10.1074/jbc.M204810200
81. Jia XY, Chang Y, Wei F, Dai X, Wu YJ, Sun XJ, Xu S, Wu HX, Wang C, Yang XZ, Wei W (2019) CP-25 reverses prostaglandin E4 receptor desensitization-induced fibroblast-like synoviocyte dysfunction via the G protein-coupled receptor kinase 2 in autoimmune arthritis. Acta Pharmacol Sin. https://doi.org/10.1038/s41401-018-0196-2
82. Bacou E, Haurogne K, Allard M, Mignot G, Bach JM, Herve J, Lieubeau B (2017) beta2-adrenoreceptor stimulation dampens the LPS-induced M1 polarization in pig macrophages. Dev Comp Immunol 76:169–176. https://doi.org/10.1016/j.dci.2017.06.007
83. Grailer JJ, Haggadone MD, Sarma JV, Zetoune FS, Ward PA (2014) Induction of M2 regulatory macrophages through the beta2-adrenergic receptor with protection during endotoxemia and acute lung injury. J Innate Immun 6(5):607–618. https://doi.org/10.1159/000358524
84. Keranen T, Hommo T, Moilanen E, Korhonen R (2017) beta2-receptor agonists salbutamol and terbutaline attenuated cytokine production by suppressing ERK pathway through cAMP in macrophages. Cytokine 94:1–7. https://doi.org/10.1016/j.cyto.2016.07.016
85. Patial S, Saini Y, Parvataneni S, Appledorn DM, Dorn GW 2nd, Lapres JJ, Amalfitano A, Senagore P, Parameswaran N (2011) Myeloid-specific GPCR kinase-2 negatively regulates NF-kappaB1p105-ERK pathway and limits endotoxemic shock in mice. J Cell Physiol 226(3):627–637. https://doi.org/10.1002/jcp.22384
86. Peregrin S, Jurado-Pueyo M, Campos PM, Sanz-Moreno V, Ruiz-Gomez A, Crespo P, Mayor F Jr, Murga C (2018) Phosphorylation of p38 by GRK2 at the docking groove unveils a novel mechanism for inactivating p38MAPK. Curr Biol 28(15):2513. https://doi.org/10.1016/j.cub.2018.07.033
87. Willemen HL, Eijkelkamp N, Garza Carbajal A, Wang H, Mack M, Zijlstra J, Heijnen CJ, Kavelaars A (2014) Monocytes/macrophages control resolution of transient inflammatory pain. J Pain 15(5):496–506. https://doi.org/10.1016/j.jpain.2014.01.491
88. Patial S, Luo J, Porter KJ, Benovic JL, Parameswaran N (2009) G-protein-coupled-receptor kinases mediate TNFalpha-induced NFkappaB signalling via direct interaction with and phosphorylation of IkappaBalpha. Biochem J 425(1):169–178. https://doi.org/10.1042/BJ20090908
89. Palikhe S, Ohashi W, Sakamoto T, Hattori K, Kawakami M, Andoh T, Yamazaki H, Hattori Y (2019) Regulatory role of GRK2 in the TLR signaling-mediated iNOS induction pathway in microglial cells. Front Pharmacol 10:59. https://doi.org/10.3389/fphar.2019.00059
90. Kawakami M, Hattori M, Ohashi W, Fujimori T, Hattori K, Takebe M, Tomita K, Yokoo H, Matsuda N, Yamazaki M, Hattori Y (2018) Role of G protein-coupled receptor kinase 2 in oxidative and nitrosative stress-related neurohistopathological changes in a mouse model of sepsis-associated encephalopathy. J Neurochem 145(6):474–488. https://doi.org/10.1111/jnc.14329